The Solar Neighborhood. XXXIX. Parallax Results from the CTIOPI and NOFS Programs: 50 New Members of the 25 Parsec White Dwarf Sample

John P. Subasavage[1,8], Wei-Chun Jao[2,8], Todd J. Henry[3,8], Hugh C. Harris[1], Conard C. Dahn[1], P. Bergeron[4], P. Dufour[4], Bart H. Dunlap[5], Brad N. Barlow[6], Philip A. Ianna[3,8], Sébastien Lépine[2], Steven J. Margheim[7]

ABSTRACT

We present 114 trigonometric parallaxes for 107 nearby white dwarf (WD) systems from both the Cerro Tololo Inter-American Parallax Investigation (CTIOPI) and the U. S. Naval Observatory Flagstaff Station (NOFS) parallax programs. Of these, 76 parallaxes for 69 systems were measured by the CTIOPI program and 38 parallaxes for as many systems were measured by the NOFS program. A total of 50 systems are confirmed to be within the 25 pc horizon of interest. Coupled with a spectroscopic confirmation of a common proper motion companion to a *Hipparcos* star within 25 pc as well as confirmation parallax determinations for two WD systems included in the recently released *Tycho Gaia* Astrometric Solution (TGAS) catalog, we add 53 new systems to the 25 pc WD sample — a 42% increase. Our sample presented here includes four strong candidate halo systems, a new metal-rich DAZ WD, a confirmation of a recently discovered nearby short-period (P = 2.85 hr) double degenerate, a WD with a new astrometric perturbation (long period, unconstrained with our data), and a new triple system where the WD companion main-sequence star has an astrometric perturbation (P $\sim$ 1.6 yr).

Subject headings: astrometry — Galaxy: evolution — solar neighborhood — stars: distances — white dwarfs

1. Introduction

White dwarfs (WDs) are the remarkably abundant remnants of the vast majority of stars and serve as reliable tracers for a number of astrophysically interesting topics. We aim to compile a robust, volume-limited sample of WDs upon which statistical studies can be performed. For instance, insight into population membership percentages (thin disk, thick disk, halo), population ages, and Galactic star formation history can be ascertained from the sample as a whole. Individually, a non-trivial number of WDs are found to be metal-enriched and are most likely displaying signs of disrupted planetary systems (Farihi et al. 2009, and reference therein). Given that the nearest metal-enriched WDs are the brightest examples, they can be more carefully studied. With a volume-limited sample, one minimizes biases in the WD luminos-

[1]U.S. Naval Observatory, 10391 West Naval Observatory Road, Flagstaff, AZ 86005-8521, USA; jsubasavage@nofs.navy.mil

[2]Department of Physics and Astronomy, Georgia State University, Atlanta, GA, 30302-4106, USA

[3]RECONS Institute, Chambersburg, PA 17201, USA

[4]Département de Physique, Université de Montréal, C.P. 6128, Succ. Centre-Ville, Montréal, Québec H3C 3J7, Canada

[5]University of North Carolina at Chapel Hill, Dept. of Physics and Astronomy, Chapel Hill, NC, 27599, USA

[6]Department of Physics, High Point University, One University Parkway, High Point, NC, 27268, USA

[7]Gemini Observatory, Southern Operations Center, Casilla 603, La Serena, Chile

[8]Visiting astronomer, Cerro Tololo Inter-American Observatory, National Optical Astronomy Observatory, which are operated by the Association of Universities for Research in Astronomy, under contract with the National Science Foundation.

ity function, mass function, and those introduced when inferring the number of planetary systems around WDs.

We present here a compilation of two long-term astrometric efforts to measure accurate trigonometric parallaxes to nearby WDs — the Cerro Tololo Inter-American Observatory Parallax Investigation (CTIOPI, Jao et al. 2005) and the U.S. Naval Observatory Flagstaff Station (NOFS, Monet et al. 1992) parallax program. In total, 76 parallaxes are measured for 69 systems by the CTIOPI program and 38 parallaxes are measured for as many systems by the NOFS program, including seven systems for which both CTIOPI and NOFS measured parallaxes. The CTIOPI results represent all completed parallaxes for WDs on the program, including those beyond the 25 pc horizon of interest. A subset of the CTIOPI targets are members of the 15 pc Astrometric Search for Planets Encircling Nearby Stars (ASPENS, Koerner et al. 2003) initiative. These targets typically have ∼10+ years of data and will be continually monitored as long as the program will allow. The NOFS parallaxes only include those within the 25 pc horizon of interest. A much larger sample of WD parallaxes from NOFS at all distances will be included in an forthcoming publication.

The combined astrometric efforts add 50 WD systems to the 25 pc sample (27 from CTIOPI, 20 from NOFS, and 3 measured by both programs). Also, we spectroscopically confirmed a previously unknown WD companion to a main-sequence dwarf with a *Hipparcos* parallax placing the system within 25 pc. Finally, we confirm proximity for two WDs whose trigonometric parallaxes were also recently determined by the *Tycho Gaia* astrometric solution (TGAS, Lindegren et al. 2016). Thus, a total of 53 new systems are added to the 25 pc WD sample that previously consisted of 126 systems reliably within that volume — a 42% increase. The complete sample of WDs within 25 pc can be found at `http://www.DenseProject.com`.

2. Observations and Data

2.1. Photometry

2.1.1. Optical BVRI Photometry

Standardized photometric observations were carried out at three separate telescopes. The SMARTS 0.9m telescope at CTIO was used during CTIOPI observing runs when conditions were photometric. A Tektronics 2K × 2K detector was used in region-of-interest mode centered on the central quarter of the full CCD producing a field of view (FOV) of $6\farcm8 \times 6\farcm8$. The SMARTS 1.0m telescope at CTIO was used with the Y4KCam 4K × 4K imager, producing a $19\farcm7 \times 19\farcm7$ FOV. Finally, the Ritchey 40-in telescope at USNO Flagstaff Station was used with a Tektronics 2K × 2K detector with a $20\farcm0 \times 20\farcm0$ FOV. Calibration frames (biases, dome and/or sky flats) were taken nightly and used to perform basic calibrations of the science data using standard IRAF packages. Standard stars from Graham (1982) and Landolt (1992, 2007, 2013) were taken nightly through a range of airmasses to calibrate fluxes to the Johnson-Kron-Cousins system and to calculate extinction corrections. In general, aperture photometry was performed on both standard stars and target stars using a $14''$ diameter. For crowded fields, faint targets, and recent observations, once a PSF pipeline was in place, PSF photometry was conducted using either the *DAOPhot* (Stetson 1987) or the *PSFEx* (Bertin 2011) algorithm. A subset of data were compared using both PSF algorithms and no significant systematic offset was seen. While three separate Johnson-Kron-Cousins VRI filter sets were used between the three telescopes, comparisons were made of dozens of CTIOPI targets mutually observed with all filter sets. Any systematic variation inherent in the filter set differences once standardized is well below our nominal magnitude error of 0.03 mag.

For the CTIOPI program, relative brightnesses were also recorded for the parallax target (hereafter referred to as the "PI" star) compared to the astrometric reference field stars in the filter used for the astrometry as part of the CTIOPI reduction pipeline. From these data, we gauge whether the PI star shows any variability. If any of the reference stars show variability above ∼2%, they are removed from the variability analysis. This anal-

ysis was not performed for the NOFS targets as it was not part of the reduction pipeline. Photometry values are given in Table 1, where columns (1) and (2) give WD and alternate names, respectively. Columns (3-10) give the Johnson BV, Kron-Cousins RI, and corresponding number of observations in each filter. Columns (11-14) give the filter of parallax observations (hereafter referred to as the parallax filter) and PI star photometric standard deviation in that filter as a gauge for variability as well as the number of nights and frames used for the variability analysis. Columns (15-17) give the JHK_s photometry values and corresponding errors on the 2MASS photometric system. Finally, column (18) contains any notes.

2.1.2. NEWFIRM JHK Photometry

Near-IR JHK_s photometry was collected for WD 0851−246, at the CTIO 4.0-m Blanco telescope using the NOAO Extremely Wide-Field Infrared Imager (NEWFIRM, Probst et al. 2004) during an engineering night on 2011.27 UT. NEWFIRM is a 4K × 4K InSb mosaic that provides a $28' \times 28'$ FOV on the Blanco telescope. Raw data were processed using the NEWFIRM science reduction pipeline and retrieved from the NOAO science archive as fully processed, stacked images.

Relative photometry was performed using the 2MASS catalog to standardize the images. Frames were checked to identify where saturation occurs and comparison stars were selected to have high signal-to-noise yet below saturation. A total of 68 comparison stars were used for each frame with 2MASS magnitudes ranging from 12.61-14.42, 12.24-13.99, and 12.14-13.90 for J, H, and K_s, respectively. The NEWFIRM filters are on the MKO system so the comparison stars were transformed to the MKO system using the methodology of Carpenter (2001)[1]. Instrumental PSF photometry was extracted using *PSFEx* for the comparison stars and the target. A least-squares fit was used to determine the offset between instrumental J and MKO J. A similar approach was used to determine the MKO $J - H$ and $J - K$ colors. Photometry values and errors are listed in Table 1 and are italicized to distinguish them from other JHK_s values on the 2MASS photometric system.

[1]The MKO transformations were not included in Carpenter (2001) but were added later and available at `http://www.astro.caltech.edu/~jmc/2mass/v3/transformations/`.

2.1.3. Catalog Photometry

Additional photometry values were extracted from the Sloan Digital Sky Survey (SDSS) DR12 (Alam et al. 2015), 2MASS, and the UKIRT Infrared Sky Survey (UKIDSS) DR9 Large Area Survey, when available. The UKIDSS project is outlined in Lawrence et al. (2007). UKIDSS uses the UKIRT Wide Field Camera (WFCAM; Casali et al. 2007). The photometric system is described in Hewett et al. (2006), and the calibration is described in Hodgkin et al. (2009). The science archive is described in Hambly et al. (2008). UKIDSS magnitudes were transformed to the 2MASS system using the transformations of Hodgkin et al. (2009). These transformed values are listed in Table 1. We do not tabulate the photometry extracted from SDSS DR12 as those are readily available via the SDSS archive.

2.2. Spectroscopy

Two WDs presented here (WD 1743−545 and WD 2057−493) are newly discovered nearby WDs identified during a spectroscopic survey of WD candidates in the southern hemisphere (Subasavage et al. in preparation) taken from the SUPERBLINK catalog (Lépine & Shara 2005). A third WD included here (WD 2307−691) was previously unclassified, yet is a common proper motion companion to a *Hipparcos* star within 25 pc (HIP 114416). A fourth WD (WD 2028−171) was suspected to be a WD by the authors based on a trawl of the New Luyten Two Tenths (NLTT) catalog (Luyten 1979a). Finally, A fifth WD (WD 1241−798) was first spectroscopically identified as a WD by Subasavage et al. (2008) but with an ambiguous spectral type of DC/DQ. The SOAR 4-m telescope with the Goodman spectrograph was used for spectroscopic follow-up as part of a larger spectroscopic campaign to identify nearby WDs to be released in a future publication. Observations were taken with a 600 lines-per-mm VPH grating with a $1''.0$ slit width to provide 2.1 Å resolution in wavelength range of 3600Å−6200Å. The slit was rotated to the parallactic angle to prevent any color-differential loss of light. For WD 1241−798, the spectrum was taken during an engineering night and only quartz lamp flats were

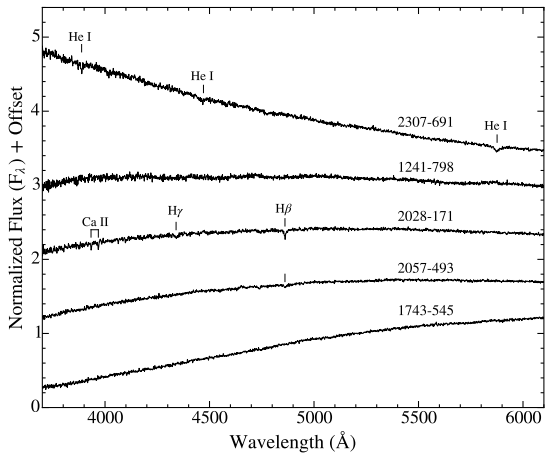

Fig. 1.— SOAR + Goodman confirmation spectra for newly discovered nearby WDs, WD 2307−691 (DB), WD 1241−798 (DC), WD 2028−171 (DAZ), WD 2057−493 (DA) and WD 1743−545 (DC). Spectra are normalized at 5200 Å and offset for clarity. Supplemental data file of these spectra is available in the online journal.

taken. The undulations seen in the spectrum correlate with structure of the quartz lamp and are thus not real. For these spectra and throughout this work, we adopt the WD spectral classification system of Sion et al. (1983). In brief, DA WDs contain Balmer features, DB WDs contain helium features, DC WDs are featureless, and DZ and DQ show calcium and carbon features, respectively, and are devoid of hydrogen and helium features. If metal features are present as well as hydrogen and/or helium features, the dominant species is listed first, i.e., DAZ is a hydrogen-dominant atmosphere with traces of calcium. The spectra for WD 1241−798 (DC), WD 1743−545 (DC), WD 2028−171 (DAZ), WD 2057−493 (DA), and WD 2307−691 (DB), normalized at 5200Å, are shown in Figure 1.

2.3. Astrometry

2.3.1. CTIOPI Astrometry

Trigonometric parallax data acquisition and reduction techniques for the CTIOPI program are discussed fully in Jao et al. (2005). In brief, the instrument setup and basic data calibrations are identical to those used for photometric observations (i.e., the SMARTS 0.9m telescope coupled with the central quarter of a Tektronics 2K × 2K detector). A parallax target's reference field is determined upon first observation. We use one of the Johnson-Kron-Cousins VRI filters, selected to optimize the signal on the PI star and reference stars (the parallax filter), as well as to keep exposure times greater than ∼30 seconds and less than ∼600 seconds, when possible. Rapid variations in the atmosphere are not "smoothed" out in short exposures and thus degrade the centroids. Integrations longer than 600 seconds are taxing to the program as a whole as we typically have ∼300-500 active targets at any given time. In general, five frames are taken at each epoch for shorter-exposure targets and three frames per epoch for 600-second-exposure targets. WD 0222−291 (see Section 4.2) is one of the faintest targets in the parallax filter observed during the program and required ∼900 second integrations. In this case, only two frames per epoch (at most) were taken.

When possible, the PI star is placed as close to the center of the CCD as possible, to allow a roughly circular distribution of reference stars around the PI star. Preference in reference star selection is given to better exposed (though not near saturation), isolated stars that are near to the PI star on the CCD. A minimum of five to ten reference stars is preferred, up to a maximum of ∼20 reference stars that are sufficiently exposed. Diminishing returns are quickly realized if more reference stars are used, often because they are poorly exposed. Exceptions are made for sparse fields when necessary, typically at the expense of a slightly degraded parallax solution. Once determined, the pointing to each field is repeated to better than ∼5-10 pixels throughout the duration of the parallax observations to minimize any CCD distortion effects on the final astrometric solution. Generally, observations are limited to within an hour angle of 2 hours, with most observations taken within ∼30 minutes of the meridian.

Astrometric reductions for each parallax target are performed/updated routinely to monitor progress and identify any problematic datasets. Centroids for the reference field and PI stars are determined for all frames in the parallax filter using *SExtractor* (Bertin & Arnouts 1996) outputs XWIN_IMAGE and YWIN_IMAGE. Corrections for differential color refraction (DCR) are per-

formed using the VRI photometry of all the reference stars and PI star. A least-squares reduction via the Gaussfit program (Jefferys et al. 1988) is performed, assuming the reference star grid has $\Sigma\pi_i = 0$ and $\Sigma\mu_i = 0$, where π and μ are parallax and proper motion, respectively. Once a relative parallax is obtained for the PI star, a correction to absolute parallax is determined by estimating photometric distances via the relations of Henry et al. (2004) to the reference stars (assuming all are dwarfs).

For three stars, WD 1241−798, WD 1620−391, and WD 1917−077, that reside within 20° of the Galactic Plane and exhibit significantly reddened fields, we performed a more rigorous calculation to correct from relative to absolute parallax. The methodology is discussed fully in Harris et al. (2016) but in brief, the reddening of the field is estimated using E($B - V$) taken from Schlafly & Finkbeiner (2011). Near infrared 2MASS photometry is used to determine which reference stars are likely giants, and the $V - I$ color is then adjusted iteratively as a distance estimate converges for each reference star, assuming a dwarf or giant. In the case of WD 1241−798, the correction to absolute parallax is determined to be 1.1 ± 0.3 mas and for the latter two, the correction is determined to be 1.6 ± 0.2 mas.

Cracked V Filter

A complete discussion of the cracked V filter issue can be found in Subasavage et al. (2009); here we give a synopsis. Because of a damaged Tek 2 V filter (referred to as oV) that occurred in early 2005, the CTIOPI program used a comparable V filter (referred to as nV) from 2005 to mid-2009. The astrometry is affected by this change because the passbands were slightly different. It was determined empirically that trigonometric parallax determinations are sound if at least ∼1-2 years of data are available both before and after the filter switch. However, subtle signals from a perturbing companion, would not be reliable. In 2009, it was determined that the crack, near the corner of the filter did not impact the FOV of the CTIOPI data, as only the central quarter of the CCD is used. Thus, a switch back to the original V (oV) was completed in mid-2009.

For the targets, particularly in the ASPENS 15 pc sample where we want to probe for subtle astrometric signatures in the residuals, the nV data are omitted from the reductions presented here. Otherwise, reductions that include both V filter data are noted in Table 2. In the case of WD 1241−798, no new data were taken after 2009 and only a year of data were taken with oV prior to 2005. Thus, only the nV data are used to determine the astrometric results presented here.

2.3.2. NOFS Astrometry

A thorough discussion of the NOFS astrometric reductions can be found in Monet et al. (1992) and Dahn et al. (2002) with procedural updates described in Dahn et al. (2017, in preparation). Briefly, astrometric data have been collected with the Kaj Strand 61-in Astrometric Reflector (Strand 1964) using three separate CCDs over the multiple decades that NOFS has measured stellar parallaxes. Initially, a Texas Instruments (TI) 800 × 800 (TI800) CCD, followed by a Tektronics 2048 × 2048 (Tek2K) CCD, and most recently an EEV (English Electric Valve, now e2v) 2048 × 4096 (EEV24) CCD were used. The latter two cameras are still in operation at NOFS for astrometric work and were used for all but two of the NOFS parallaxes presented here. The TI800 CCD was used to measure the parallaxes for WD 0213+396 and WD 1313−198. A total of four filters were used for astrometric work. ST-R (also known as STWIDER) is described in detail by Monet et al. (1992), and is centered near 700 nm with a FWHM of 250 nm. A2-1 is an optically flat interference filter centered near 698 nm with a FWHM of 172 nm. I-2 is an optically flat interference filter centered near 810 nm with a FWHM of 191 nm. Z-2 is an optically flat 3 mm thick piece of Schott RG830 glass that produces a relatively sharp blue-edge cutoff near 830 nm and for which the red edge is defined by the CCD sensitivity. More details on the filters can be found in Dahn et al. (2017, in preparation).

Reference stars are selected during initial setup, typically with more selections than required. Centroids for the reference field and PI star occur on-the-fly as data are collected using the centroiding algorithm of Monet & Dahn (1983). A comparison of this algorithm and that of *SExtractor* as used for CTIOPI, using several parallax fields, show them to produce comparable results. Corrections for

DCR were determined based on the $V - I$ colors and applied to the PI and reference star centroids prior to the astrometric solution. An astrometric solution is then calculated to give relative parallax and proper motion.

The correction to absolute parallax is determined using the methodology of Harris et al. (2016) and the same as that described for the reddened cases in the CTIOPI program. Corrections for most of the targets presented here do not require the use of 2MASS photometry to determine reference stars likely giants vs. dwarfs, as reddening is minimial. The correction to absolute for WD 1821−131 was not determined in this manner because the Schlafly & Finkbeiner (2011) determination of $E(B - V) = 13.9$ for this field and thus, giant/dwarf differentiation was very unreliable. Instead, we adopt a nominal correction with an inflated error of 1.0 ± 0.3 mas for this target.

3. Astrometry Results

CTIOPI astrometric results for WD systems (and companions when available) are presented in Table 2. Columns (4)-(9) list the filter used for parallax observations, the number of seasons the PI star was observed, the total number of frames used in the parallax reduction, the time coverage of the parallax data, and the number of reference stars used. The 'c' in column (5) signifies that the observations were continuous throughout every season within the time coverage. The 's' signifies that observations were scattered such that there is at least one season with only one night's data (or no data for an entire season). In some cases, mostly because of the cracked V filter problem discussed in Section 2.3.1, the 'g' signifies a significant gap (multiple years) in the observations. Columns (10)-(12) list the relative parallax, correction to absolute, and the absolute parallax. The proper motions and position angles quoted in columns (13) and (14) are those measured with respect to the reference field (i.e., relative, not corrected for reflex motion due to the Sun's movement in the Galaxy). The tangential velocities quoted in column (15) are not corrected for solar motion. For the ASPENS targets that were published by Subasavage et al. (2009), continual monitoring over the past ∼6 years has provided significant additional data, and thus the astrometric results presented here supersede those previously published. The mean error on the parallax for the CTIOPI sample is 1.14 mas.

NOFS astrometric results for 25 pc WD systems are presented in Table 3. Columns (4)-(9) list the filter used for parallax observations, the number of nights the PI star was observed, the total number of frames in the astrometric reduction, the number of reference stars used, and the time coverage and length of the parallax data. Columns (10)-(14) list the relative parallax, correction to absolute, the absolute parallax, and relative proper motion and position angle (i.e., not corrected for solar motion). Also in this case, the tangential velocities quoted in column (15) are not corrected for solar motion. Finally, column (16) denotes which camera was used for parallax observations. The mean error on the parallax for the NOFS sample is 0.49 mas, or roughly a factor of two better than that for CTIOPI. The enhanced accuracy is attributed to the astrometric optimization of the NOFS 61-in Strand Reflector's optical design.

In Figure 2 we compare astrometric results with recently published works for the few overlapping targets. The error bars represent both programs' formal parallax errors added in quadrature for a given target. There are no obvious systematic differences with either CTIOPI or NOFS samples.

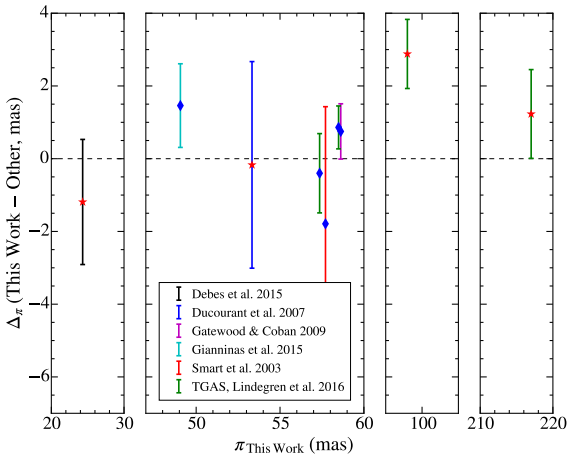

Fig. 2.— Comparison of trigonometric parallax results with other authors' recent results, shown as $\Delta\pi$ (this work − other). Comparisons with CTIOPI are shown as red stars and with NOFS as blue diamonds.

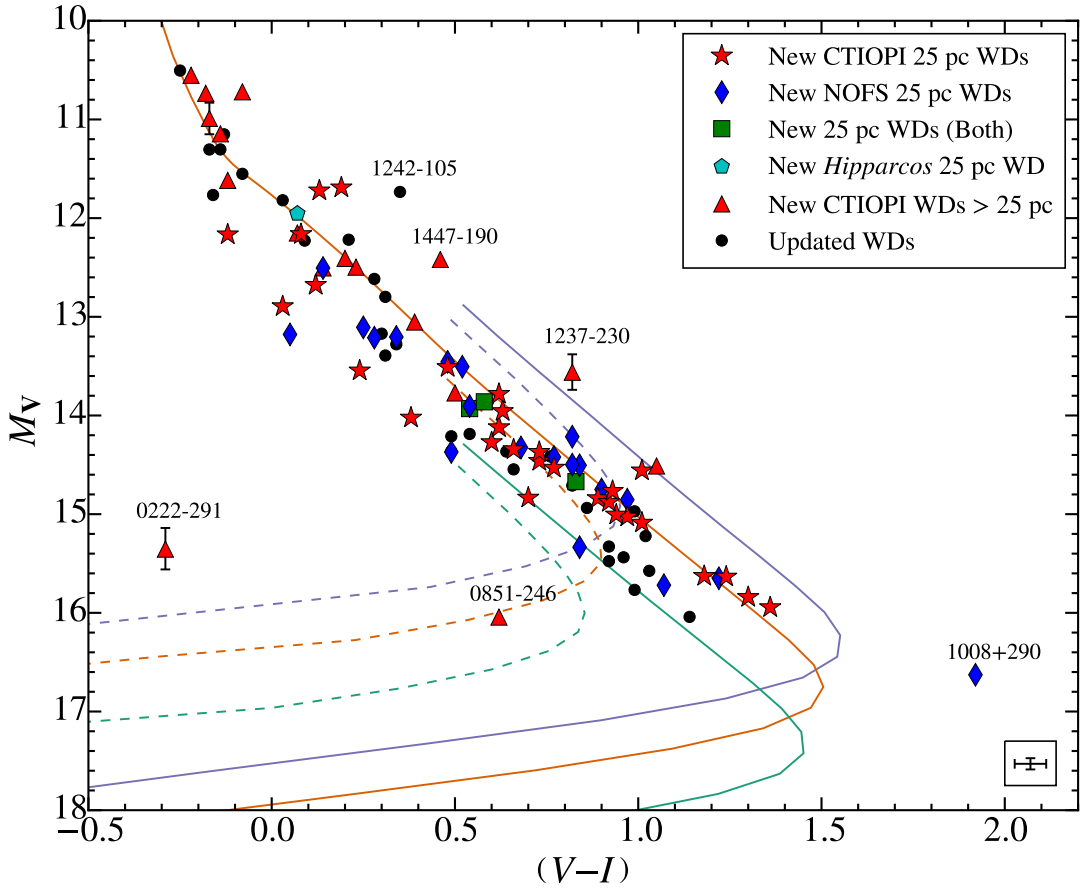

Fig. 3.— Hertzsprung-Russell diagram for the objects with parallaxes presented here, separated by sample. For the CTIOPI sample, objects beyond 25 pc are included as red triangles. Objects labeled by WD name are discussed in Section 4.2. A representative error bar is encased in the lower right corner of the plot. Error bars are plotted explicitly for the three objects whose M_V errors are larger than 0.15 mag. Curves represent atmospheric model tracks for three values of log g , 7.5 (*purple*), 8.0 (*orange*), and 8.5 (*green*). Solid curves are pure-H models and the dashed curves are mixed atmosphere He+H models of Bergeron et al. (1995), with improvements discussed in Tremblay & Bergeron (2009), with log [He/H] = 2.0. All other reasonable mixed atmosphere models fall between these two curves of a given log g . For all models other than the pure-H model at log g = 8.0, curves are plotted for $T_{\rm eff}$ = 7,000K and cooler.

Figure 3 shows a H−R diagram for the astrometric samples presented here. Objects labeled by WD name are discussed in detail in Section 4.2. Briefly, we find three WDs (WD 1242−105, WD 1447−190, and WD 1237−230) that are overluminous and good candidates for being unresolved multiple systems solely based on luminosity. WD 1008+290 is a peculiar He-rich DQ WD with exceptional Swan band absorption (e.g., Giammichele et al. 2012) such that the measured V magnitude, whose bandpass encompasses a portion of this absorption, is affected and appears fainter than if the absorption was not present. Finally, both LHS 2068 (WD 0851−246) and LHS 1402 (WD 0222−291) are very cool WDs that appear to display collision-induced absorption (CIA) by H_2 molecules (Saumon et al. 1994; Hansen 1998; Saumon & Jacobson 1999). CIA opacity is induced by collisions, and thus requires high atmospheric pressures. High atmospheric pressures are reached at much higher effective temperatures in He-rich atmospheres that also contain molecular hydrogen, because of the relative transparency of He, than in pure-H atmospheres. Therefore, CIA manifests itself at higher effective temperatures, and thus higher luminosities. This effect is

shown in Figure 3 compared to the effect of CIA in pure-H atmospheres. In the case of LHS 2068, a mixed atmosphere He+H is required to allow for CIA to be present at its luminosity (discussed further in Section 4.2). In the case of LHS 1402, none of the current models compare adequately to the observed data (also discussed further in Section 4.2). As expected, the majority of new 25 pc WD members are cooler and intrinsically dimmer than their hotter counterparts and often missed in magnitude-limited surveys.

4. Analysis

4.1. Modeling of Physical Parameters

To better understand the physical nature of WDs, which expands to provide clues into topics such as stellar evolution and progenitor populations, for example, we perform atmospheric modeling analyses of all of our targets. Atmospheric modeling procedures of the WDs are identical to those presented in Subasavage et al. (2009). Briefly, optical/near-IR magnitudes are converted into fluxes using the calibration of Holberg et al. (2006) and compared to the spectral energy distributions (SEDs) predicted by the model atmosphere calculations originally described in Bergeron et al. (1995, and references therein) with improvements discussed in Tremblay & Bergeron (2009). The observed flux, f_λ^m, is related to the model flux by the equation

$$f_\lambda^m = 4\pi\ (R/D)^2\ H_\lambda^m \qquad (1)$$

where R/D is the ratio of the radius of the star to its distance from Earth, H_λ^m is the Eddington flux (dependent on $T_{\rm eff}$, log g , and atmospheric composition) properly averaged over the corresponding filter bandpass, and π is the mathematical constant (elsewhere throughout this paper, π refers to the trigonometric parallax angle). Our fitting technique relies on the nonlinear least-squares method of Levenberg-Marquardt (Press et al. 1992), which is based on a steepest descent method. The value of χ^2 is taken as the sum over all bandpasses of the difference between both sides of Equation (1), weighted by the corresponding photometric uncertainties. Only $T_{\rm eff}$ and $[\pi(R/D)^2]$ are free parameters (though we allow log g to vary as described below) and the uncertainties of both parameters are obtained directly from the covariance matrix of the fit. The main atmospheric constituent (hydrogen or helium) is determined by the presence of Hα from spectra published in the literature (references listed in Table 4) or by comparing fits obtained with both compositions.

We start with log g = 8.0 and determine $T_{\rm eff}$ and $[\pi(R/D)^2]$, which combined with the distance D obtained from the weighted mean trigonometric parallax measurement yields directly the radius of the star R. The radius is then converted into mass using evolutionary models similar to those described in Fontaine et al. (2001), but with C/O cores, $q({\rm He}) \equiv \log M_{\rm He}/M_\star = 10^{-2}$ and $q({\rm H}) = 10^{-4}$ (representative of hydrogen-atmosphere WDs), and $q({\rm He}) = 10^{-2}$ and $q({\rm H}) = 10^{-10}$ (representative of helium-atmosphere WDs).[2] In general, the log g value obtained from the inferred mass and radius ($g = GM/R^2$) will be different from our initial guess of log g = 8.0, and the fitting procedure is thus repeated until an internal consistency in log g is reached. The parameter uncertainties are obtained by propagating the error of the trigonometric parallax measurements into the fitting procedure.

Physical parameter determinations for the DQ and DZ WDs are identical to the procedures outlined in Dufour et al. (2005, 2007). Briefly, the photometric SED provides a first estimate of the atmospheric parameters with an assumed value of metal abundances using solar abundance ratios. The optical spectrum is fit to better constrain the metal abundances and to improve the atmospheric parameters from the photometric SED. This procedure is iterated until a self-consistent photometric and spectroscopic solution is reached.

Results of the atmospheric modeling are tabulated in Table 4. Given the nominal uncertainties, we round the values for effective temperature and corresponding error to 10 K. Representative plots of the model fits of the SEDs are shown in Figure 4, with the complete set of plots for the entire sample made available in the online material.

4.2. Comments on Individual Systems

WD 0000−345 belongs to an unusual class of objects whose SEDs are better fit with pure-H at-

[2] see `http://www.astro.umontreal.ca/~bergeron/CoolingModels/`.

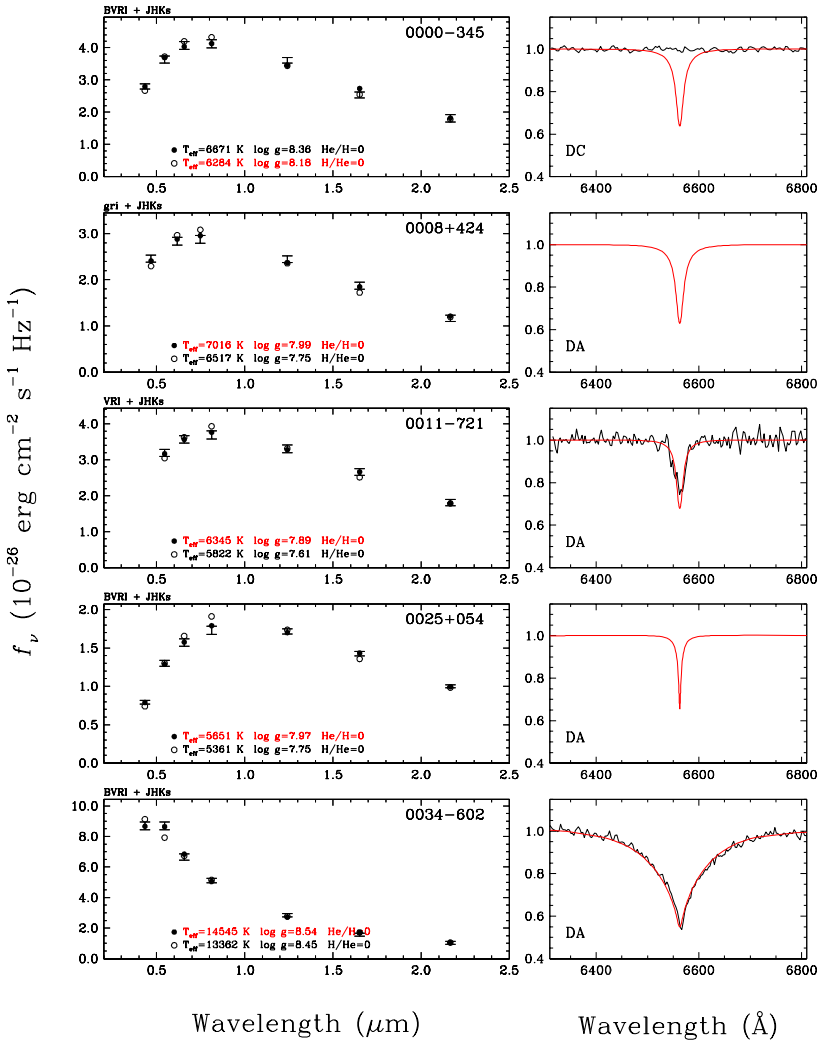

Fig. 4.— Representative plots of the model fits to the SEDs where error bars represent measured values and circles represent model values (filled for pure-H and open for pure-He). Adopted model parameters are shown in red text in the left panels. Plots of all model fits for the sample are available in the online material. Among the online plots, note that both WD 0038−226 and WD 0851−246 are fit using mixed-atmosphere He+H models. All photometric measures that were excluded from the fit are shown as red error bars and described in Section 4.2. Model spectra in the right panels are not fits, but merely derived from the adopted model atmospheres assuming pure-H. Comparisons with measured spectra (black lines), when available, are shown and serve as consistency checks for the DA WDs and to highlight any anomalies. Fits for DQ and DZ are plotted separately and, in these cases, spectral fitting is performed as described in Section 4.1.

mospheric models, yet show no Balmer spectral features. This class was first identified by Bergeron et al. (1997) and more recently discussed in Giammichele et al. (2012), who suggest that strong magnetic fields could be the cause of the discrepancy. In fact, WD 0000−345 was initially classified as a magnetic WD by Reimers et al. (1996) and later classified as a DC by Bergeron et al. (1997). Circular polarization studies by Schmidt et al. (2001) show no detectable magnetic field, and thus we classify this object as a DC. We adopt the pure-He atmospheric models

to remain consistent with model choice based on spectroscopy, where available.

WD 0127−311 was initially classified as a magnetic WD by Reimers et al. (1996) yet circular polarization studies by Schmidt et al. (2001) show no detectable magnetic field. While the spectrum shows what appears to be He I 5876 Å, indicative of a DB, Schmidt et al. (2001) argue that other helium features at 4472 Å and 6678 Å should be present for a wide range of temperatures, yet are absent here. Schmidt et al. (2001) suggest the object could be a DZ with the Na I D lines (5890 and 5896 Å) but the spectral profile seen is asymmetric, unlike what is expected for the Na lines. We favor the former interpretation and have adopted a spectral type of DB for this object. Given that it is a rather cool DB, the He I 5876 Å line will be the last feature seen as the WD cools to a DC spectral type. In fact, this DB is of a very similar effective temperature (10,910 K) to the newly discovered DB, WD 2307−691 (also 10,910 K), whose spectrum is shown in Figure 1 and also displays a prominent He I 5876 Å feature and little else.

WD 0222−291 was first discovered to be a high proper motion star by Luyten & La Bonte (1972) (LP 885−57; LHS 1402, Luyten 1979b) with $\mu = 0.501$ ″ yr^{-1}at position angle 96.3°. It was later observed spectroscopically by Oppenheimer et al. (2001) and found to be a featureless ultracool WD with strong infrared CIA that extends into the optical bandpasses, thereby giving it significantly blue optical colors. Oppenheimer et al. (2001) postulated that WD 0222−291 was direct evidence of galactic halo dark matter (based on kinematics) along with the other 37 WDs presented in that publication. The claim of these objects being halo members was contested based on the relatively young ages of these systems (Bergeron 2003). However, there remained an ambiguity with WD 0222−291 as to whether the CIA was due to collisions with hydrogen molecules only (pure-H atmosphere) or due to collisions with neutral helium (mixed atmosphere He+H) that can produce comparable CIA at higher temperatures. The difference in luminosity between the two scenarios is significant. If a pure-H atmosphere is assumed, WD 0222−291 would be one of the nearest WDs to the Sun at 4.7 pc (Bergeron 2003). If the atmosphere is dominated by helium with only trace amounts of hydrogen, then WD 0222−291 is considerably more distant at 20 - 25 pc (Salim et al. 2004; Bergeron et al. 2005). The latter scenario was preferred because the spectrum did not exhibit a broad absorption feature near 8000 Å as expected in pure-H models (see Figure 5 of Bergeron et al. 2005).

Here we confirm, with our trigonometric distance of 34.6 ± 3.5 pc, that WD 0222−291 is indeed more consistent with a helium-dominant atmosphere with the CIA being due to trace amounts of hydrogen in this mixed atmosphere. However, we do not arrive at a satisfactory fit using any of the currently available models. The object is overluminous compared to predictions and, thus, could be a double degenerate or the current models are inadequate (or both). Therefore, we refrain from listing any physical parameters for this WD. In that regard, WD 0222−291 can serve as an important empirical test case for future atmospheric models.

We note that our parallax error is uncharacteristically large and we attribute this to three causes. First, this object is exceptionally faint so that the signal-to-noise of our CTIO 0.9m astrometry images is quite low. Second, long integration times (∼15 minutes per frame, on occasion), produced images with less-than-circular contours because of imperfect guiding. Third, fewer frames were collected because of the costly integration times and their impact on the rest of the parallax program. Nonetheless, the parallax result shows no indication of systematics resulting from these effects and the error is slightly better than 10% of the parallax measured. Indeed, over the 6+ years that parallax data were collected, the parallax value stabilized such that new data did not change the result, indicative of a robust determination.

WD 0311−649 was classified as a DA by Subasavage et al. (2008) for which they estimated a distance of 21.0 pc. The trigonometric parallax presented here implies a significantly greater distance such that the implied mass, assuming a single star, is remarkably low. This object is likely an unresolved double degenerate.

WD 0322−019 is shown by Zuckerman et al. (2003) to be a double degenerate where both components show metal lines and are thus DAZ spectral types. In addition, Farihi et al. (2011) identify a magnetic field of ∼120 kG and model the system using a preliminary parallax from USNO of 58.02

± 0.44 mas. The updated parallax presented here, which includes several years of additional data, is entirely consistent.

WD 0326−273 was confirmed by Zuckerman et al. (2003) to be a double degenerate based on radial velocity variations of $H\beta$. In addition, they find Ca II lines, but attribute the source as being interstellar given the discrepant radial velocities compared to $H\beta$.

WD 0552−041 is a weak DZ. However, as discussed in Giammichele et al. (2012), the sharp Ca II H & K lines indicate a hydrogen-rich atmosphere. If the atmosphere were helium-rich, the atmospheric pressure would be greater, and thus the Ca II line profiles would be much broader and shallower. Therefore, we utilize a pure-H model to derive the physical parameters in Table 4.

WD 0802+387 has a recent trigonometric parallax determination by Gianninas et al. (2015) of 47.6 ± 1.0 mas. Thus, their measure adds this target to the 25 pc sample, bringing the number of reliable member systems to 126 prior to this work. Our trigonometric parallax presented here is entirely consistent and is included in our number counts as an updated measure. The weighted mean of these two measures is used to calculate physical parameters shown in Table 4.

WD 0851−246 was first discovered to be a high proper motion star by Luyten (1974) (LP 844−26; LHS 2068, Luyten 1979b) with $\mu = 0\farcs630$ yr^{-1} at position angle 78.0°. It has a common proper motion companion (LHS 2067) whose spectral type is listed as sdM in Kirkpatrick et al. (1995). The WD component was first spectroscopically identified by Ruiz & Bergeron (2001), named CE 51 by those authors, during a follow-up spectroscopic campaign targeting proper motion objects detected in the Calán-ESO survey (Ruiz et al. 2001). They determine that the WD is very cool (2730 K), old (11.9 Gyr), and nearby (14.7 ± 0.3 pc). Silvestri et al. (2002) conducted a radial velocity survey of wide binaries with WD components, including this system, and found a $V_{\rm rad}$ = 0.0 ± 15.8 km/sec for the sdM. Based on the WD's location in the H-R digram (Figure 3), it is expected that CIA is present and likely results from collisions with molecular helium, thus, is a mixed atmosphere He+H. The physical parameters presented in Table 4 are derived from a mixed atmosphere model with the fit shown in Figure 4. This is the coolest WD presented here for which we were able to derive reliable atmospheric parameters. Notably, the mixed atmosphere fit results in a significantly higher $T_{\rm eff}$ (3490 K) than that found by Ruiz & Bergeron (2001).

Additionally, Kilic et al. (2009) observed this system with Spitzer in the IRAC bandpasses, but stated that contamination from a nearby bright star makes the photometry questionable. As discussed in Section 2.1.2, we obtained JHK_s photometry using NEWFIRM on the CTIO Blanco 4-m. The SED clearly shows excess in the near-IR indicative of a cool, very red tertiary companion. Follow-up observations, in particular, near-IR spectroscopy, are required to characterize the tertiary companion. The mixed atmosphere fit shown in Figure 4 excludes the JHK_s values; the optical magnitudes are not affected by this very red unseen companion.

WD 1008+290 is a peculiar DQ WD with exceptional Swan band absorption such that the measured V magnitude, whose bandpass encompasses a portion of this absorption, is affected and appears fainter than if the absorption was not present. Additionally, the $V - I$ color is inflated for the same reason resulting in the WD's displacement in Figure 3. We adopt a pure-He model atmosphere simply because there was no satisfactory agreement with the SED, regardless of model used; thus, the atmospheric parameters are likely unreliable.

WD 1036−204 is another peculiar DQ WD with exceptional Swan band absorption. We adopt a pure-He model atmosphere simply because there was no satisfactory agreement with the SED, regardless of model used, thus, the atmospheric parameters are likely unreliable.

WD 1237−230 was first discovered to be a high proper motion star by Luyten (1972) (LP 853−15; LHS 339, Luyten 1979b) with μ = 1.102″ yr^{-1}at position angle 219.9°. It was first classified as a DA WD by Liebert & Strittmatter (1977). Subasavage et al. (2007) obtained optical VRI photometry and combined it with JHK_S from 2MASS to model the SED and derive physical parameters. One significant discrepancy is the distance estimate derived (26.9 ± 4.5 pc) compared to the trigonometric distance determined in this work (39.4 ± 3.6 pc). The recent spectroscopic analysis of Kawka & Vennes (2012) showed

this object to be a single-lined binary, and they identify this object to be a candidate halo WD based on the estimated distance. Our trigonometric parallax further strengthens the case for halo membership, as it has an extreme tangential velocity of 202.4 km sec^{-1}. We see no evidence for photocentric motion in the astrometric dataset, leaving open two possibilities: (1) a system with two roughly equal-mass, equal luminosity components, or (2) a system with a period short enough (P $\lesssim$ 1 year) to evade detection in our astrometric data. Given the overluminosity in the optical (see Figure 3), such that the components are of similar brightnesses, coupled with the single-lined radial velocity variation, the system is likely composed of a DA and a non-DA pair of WDs.

WD 1241−798 was classified as a DQ/DC by Subasavage et al. (2008) without further explanation. The ambiguous spectral classification arises because the authors obtained a red spectrum from the Blanco 4-m at CTIO using the R-C Spectrograph. With a blue cutoff of ∼5500 Å, no sharp features were present, yet there were depressions very close to where the C_2 Swan bands are expected but the detection is marginal. To remove this discrepancy, we acquired a confirmation spectrum using SOAR + Goodman during an engineering night on 2017.28 UT and as described in Section 2.2. While undulations exist in the spectrum, they correlate with the internal quartz lamp used for flat fielding such that this object is of spectral type DC as shown in Figure 1. This object is similar to WD 0000−345 in that a pure-H model better fits the SED over a pure-He model, yet no Balmer features are seen in the spectrum. Thus, we use a pure-He atmospheric model to characterize this object.

WD 1242−105 was first classified as a hot subdwarf (sdB) by Kilkenny et al. (1988) and later identified as a DA WD by Vennes & Kawka (2003) who estimated a photometric distance of 18 ± 4 pc. It was then placed on the parallax program to confirm proximity. With a trigonometric parallax distance of $41.1^{+2.63}_{-2.33}$ pc, we suspected this object to be an unresolved double star.

During a spectroscopic campaign using the SOAR telescope with the Goodman spectrograph briefly described in Section 2.2, we were assisting with the commissioning of a 2100 lines-per-mm VPH grating and chose to observe this object as a test case. The observations were taken on 2011 July 22 and a slit width of 0.″84 was used to optimize spectral resolution and throughput. Spectral coverage was 3700−4400 Å with a spectral resolution of 0.8 Å pixel^{-1}. The long slit was oriented so that a bright calibrator (2MASS J12445203-1049037) was also in the slit to serve as a check for any wavelength calibration systematic uncertainties (though it was not known a priori if this calibrator was radial velocity stable). The targets were observed for ∼2 hours, taking repeated exposures of 150 seconds each. After every seven exposures, arc lamps were taken to ensure

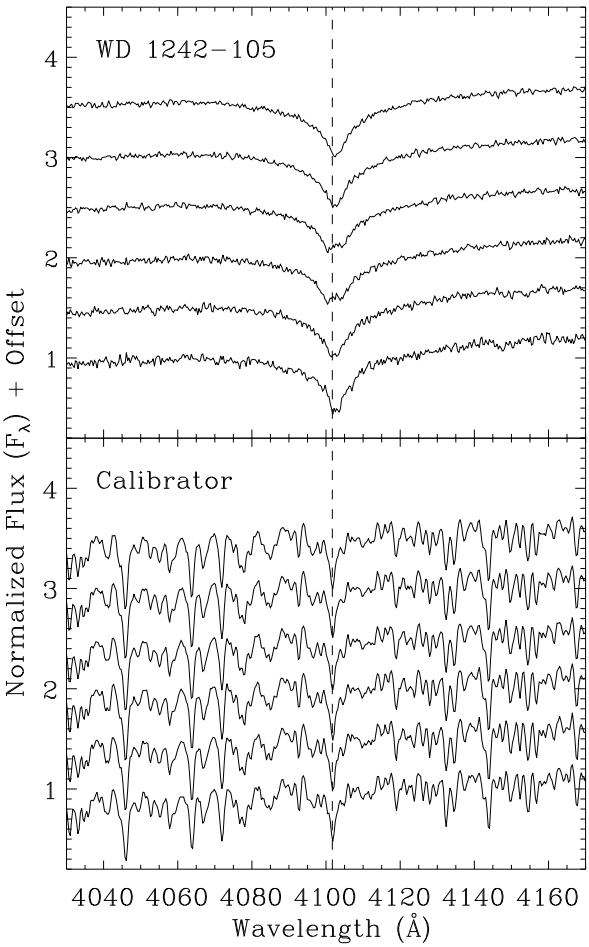

Fig. 5.— SOAR + Goodman stacked spectra for WD 1242−105 (*top panel*) and the calibrator star (*bottom panel*). The dashed vertical line denotes the location of Hβ. These spectra cover roughly half of the orbital period of WD 1242−105.

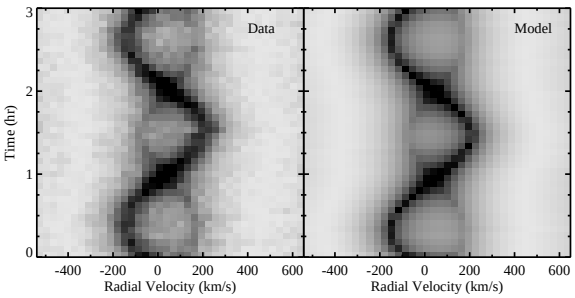

Fig. 6.— Trailed spectrogram of the Gemini-South + GMOS data for WD 1242−105 around the Hα region (*left panel*) as well as a noiseless model spectrogram using our derived radial velocity solution (*right panel*).

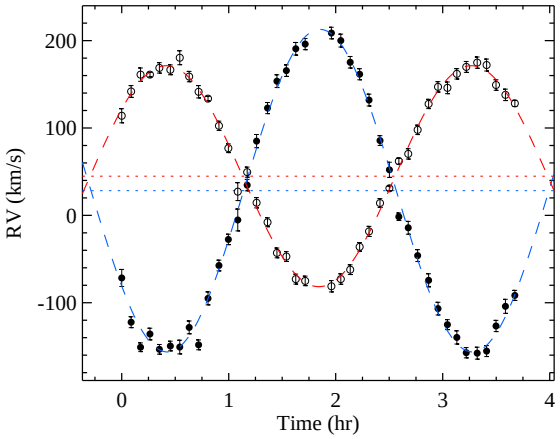

Fig. 7.— Component radial velocity curves for WD 1242−105 as a function of time. Open circles and filled circles correspond to measures for the more massive component and less massive component, respectively. The horizontal dashed lines represent the γ values with the difference between the two being a result of differing gravitational redshifts. Supplemental data file of these radial velocity measurements is available in the online journal.

accurate wavelength calibration. Spectroscopic reductions were performed using standard IRAF routines in the *Specred* package. Once wavelength calibration was performed on each spectrum (using the arc lamp taken closest in time), each block of seven spectra was stacked to increase S/N, thus resulting in a cadence of roughly 25 minutes. For consistency, the calibrator spectra were stacked in an identical manner. See Figure 5.

Once it was evident that the system was a double-lined double degenerate with rapidly changing relative velocities, we requested the use of the Gemini Multi-Object Spectrograph-South (GMOS-S) to better characterize the orbital period. Spectroscopic data were taken on 2012.31 UT using the R831_G5323 grating, centered at 6720 Å, with a slit width of 0.″25. We opted for a central wavelength somewhat distant from the targeted Hα absorption line at 6563 Å because the GMOS-S central detector suffered from a bad column just blueward of center (since been replaced). With a full wavelength coverage of 5540−7640 Å and a ∼700 Å span within each detector, the Hα region was amply sampled within the central detector (to avoid the gaps between detectors). The observing sequence consisted of a target acquisition on the slit followed by a block of five spectroscopic observations, each of 300 seconds integration. This block of five exposures, followed by an arc lamp, was repeated four times. Then, a re-acquisition was performed to ensure the target was centered in the narrow slit and the observing sequence was repeated. The observations span nearly four continuous hours and resulted in 40 science spectra. Data were reduced using the external IRAF package *Gemini* Version 1.11 and, in particular, the suite of routines in the *GMOS* subpackage. Science spectra were wavelength calibrated with the arc lamp taken nearest in time to the science spectra.

Spectral line fitting was performed as follows. The Hα absorption lines were fit at maximum separation using pseudo–Gaussian profiles to determine individual profile shapes (line depths and widths). The profile shape was then fixed and applied to all other spectra with the only free parameter being the pseudo–Gaussian centroid. Synthetic Hα spectra were then created using these best-fitting models, with the same resolution, to generate the noiseless model trailed spectrogram and compared to the data as shown in Figure 6.

These data, once fitted, revealed a double degenerate with a 2.85-hour period. The component radial velocity curves as a function of time are displayed in Figure 7. The differences in the apparent systemic velocities for each component are because of differences in component gravitational

redshifts. The vital parameters for this system are summarized in Table 5 and agree very well with those determined by Debes et al. (2015), as does our parallax determination compared to those authors' trigonometric parallax.

WD 1314−153 was shown to be, most likely, a young halo WD by Kawka & Vennes (2012) based on kinematics that include radial velocity measurements as well as tangential motions assuming a distance of 58 pc. Our trigonometric parallax distance of 58.1 pc is entirely consistent with their distance estimate and the space motions are confirmed.

WD 1339−340 was shown to be a strong halo candidate with a nearly polar Galactic orbital motion by Lépine et al. (2005). They estimate a distance of 18 pc for their analysis, entirely consistent with our trigonometric parallax distance of 21.0 pc. With a $V_{\rm tan}$ = 255.0 km sec^{-1}, this object has the largest tangential velocity of the 25 pc WD sample. Thus, space motions and strong halo candidacy are confirmed.

WD 1447−190 was first spectroscopically identified as a DA WD by Kawka & Vennes (2006). The photometric distance estimate of 29.1 ± 4.9 pc (Subasavage et al. 2007) is significantly discrepant from its trigonometric parallax distance of 47.4 ± 2.0 pc. Thus, we expected this system to be an unresolved double degenerate and it served as a second target for the commissioning of the SOAR + Goodman spectrograph using the 2100 lines-per-mm VPH grating. It was observed on three separate nights; 19 July 2011, 22 July 2011, and 6 September 2011. The instrument setup is similar to that used for the observations of WD 1242−105 and has the same wavelength coverage. The first two nights of observations used a 0.″84 slit width with the slit oriented such that a brighter star, 2MASS J14500516-1912509, was also included in the slit to act as a calibrator. The observing sequence for the first two nights consisted of four 300 second integrations followed by an arc lamp as a single block of exposures. This sequence was repeated eight, and seven times, respectively, for the first two nights. The data showed no short-period variations over the course of each night so all data for a night were stacked into a single spectrum (see Figure 8, top two spectra in each panel). The third night's data set was smaller as these observations were taken between

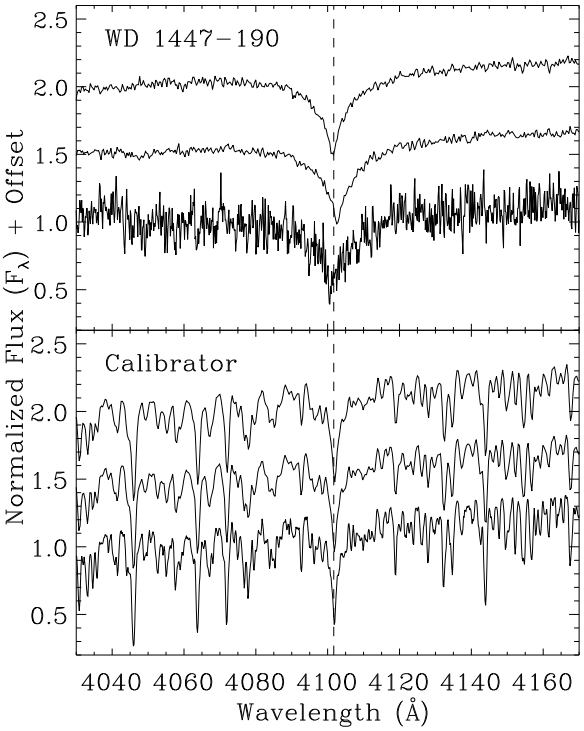

Fig. 8.— SOAR + Goodman stacked spectra for WD 1447−190 (*top panel*) and the calibrator star (*bottom panel*). The dashed vertical line denotes the location of Hβ.

core commissioning tasks. The instrument setup consisted of a 0.″46 wide slit oriented to include the same calibrator star. Pairs of 600 second exposures were taken followed by an arc lamp. This sequence was repeated twice. All data from this night were stacked into a single spectrum though are noisier than the previous two nights' spectra.

A clear single-lined radial velocity variation is seen in the WD and is shown in Figure 8. The period is unconstrained with these data but the multiplicity is confirmed. We hope to obtain spectroscopic follow-up and better characterize the orbital parameters of this system.

WD 1814+134 was first discovered by the SUPERBLINK survey as a high proper motion star (μ = 1.″207 yr^{-1}, Lépine et al. 2002) and later spectroscopically classified as a DA10 (Lépine et al. 2003). A trigonometric parallax of 70.3 ± 1.2 mas was measured by Lépine et al. (2009) from data taken between 2005.48 and 2007.72. The NOFS trigonometric parallax (presented here) of

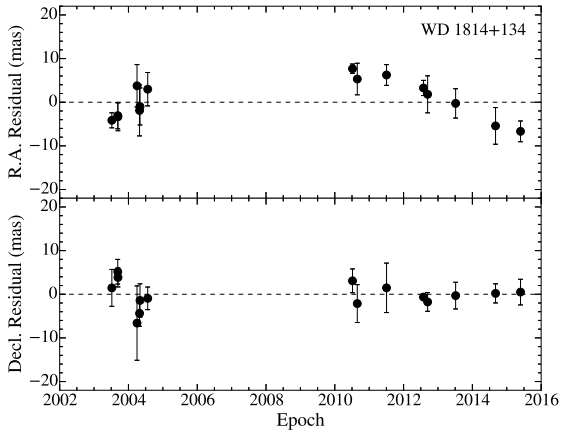

Fig. 9.— CTIOPI nightly mean astrometric residuals of WD 1814+134, once parallax and proper motion are removed, that show a long-period astrometric perturbation.

66.05 ± 0.28 mas was measured from data taken between 2008.29 and 2012.47 and only marginally agrees with the previous trigonometric parallax at the 3-σ level. A third trigonometric parallax of 68.25 ± 0.96 mas was measured by CTIOPI (also presented here) and includes data taken between 2003.52 and 2015.40, albeit with a gap from 2005 to 2010 because of the different V filter used (see Section 2.3.1). The CTIOPI dataset shows a clear, long-period astrometric perturbation, largely in the right ascension axis, though notable in the declination axis at the earliest epochs (see Figure 9). This perturbation is likely the cause for the discrepant parallax determinations from data acquired during different phases of the orbit. This target remains on the CTIOPI program, and has been re-added to the NOFS astrometric program to better characterize the perturbation. A weighted mean parallax using all three measures has been adopted for the analysis. Given that the trigonometric distance is entirely consistent with atmospheric modeled distance estimates for a single WD (e.g., Lépine et al. 2003; Subasavage et al. 2007), and there is no noticeable near-IR excess, the companion is likely to be very low-luminosity.

WD 2028−171 is a newly discovered nearby WD that was targeted for spectroscopic followup based on a trawl of the NLTT Catalog. As discussed in Section 2.2, we obtained an optical spectrum of this object and find it to show Ca II H & K lines (DAZ) indicative of metal pollution by recent/ongoing accretion. Follow-up observations are necessary to better characterize this candidate remnant planetary system.

WD 2057−493 is a newly discovered nearby WD using the SUPERBLINK database and discussed in Section 2.2. It is also a common proper motion companion to red dwarf WT 766 ($\rho = 64\farcs3$ at P.A. 340.3°, epoch = 2015.55951 – measured from CTIOPI astrometry frames) for which an independent trigonometric parallax was measured via CTIOPI. WT 766 shows a clear astrometric perturbation in the residuals consistent with a period of less than two years. The residuals were fit to an orbital model, and while most orbital parameters (e.g., eccentricity, semi-major axis) are poorly constrained with an orbital inclination near 90°, the period was well determined to be 1.648 ± 0.018 years. The orbital fit is plotted over the residuals in Figure 10 and removed from the astrometric analysis to enable a refined trigonometric parallax. The parallax determinations for WT 766 and WD 2057−493 agree very well, and thus this is a new triple system within 15 pc.

WD 2159−754 is flagged as an ultramassive WD by Kawka et al. (2007) with a mass of 1.17 $M_\odot$. They assume a distance of 14 pc for their analysis. Our trigonometric parallax distance of 19.9 pc results in a slightly lower mass (though still massive) of 0.97 $M_\odot$.

WD 2226−754AB is a widely separated double degenerate pair consisting of two cool, featureless DC WDs, originally discovered by Scholz et al. (2002). While the tangential velocity of this pair at ∼135 km sec^{-1} is only marginally consistent with halo kinematics, the calculated space motion (assuming zero tangential velocity as none has been measured) is more convincing with $V \sim -112$ km sec^{-1} (positive in the direction of Galactic rotation). Coupled with the WD cooling ages and masses for each component (A: ∼6.5 Gyr and 0.50 $M_\odot$; B: ∼7.4 Gyr and 0.51 $M_\odot$), we nominally classify this system as a strong halo candidate.

WD 2307−691 is a common proper motion companion, found at J2000 coordinates 23:10:22.96 -68:50:20.2 (epoch 2011.6966) to HIP 114416 (GJ 1280, LTT 9387), yet has not been characterized in the literature. It was brought to the authors' attention by Brian Skiff (private com-

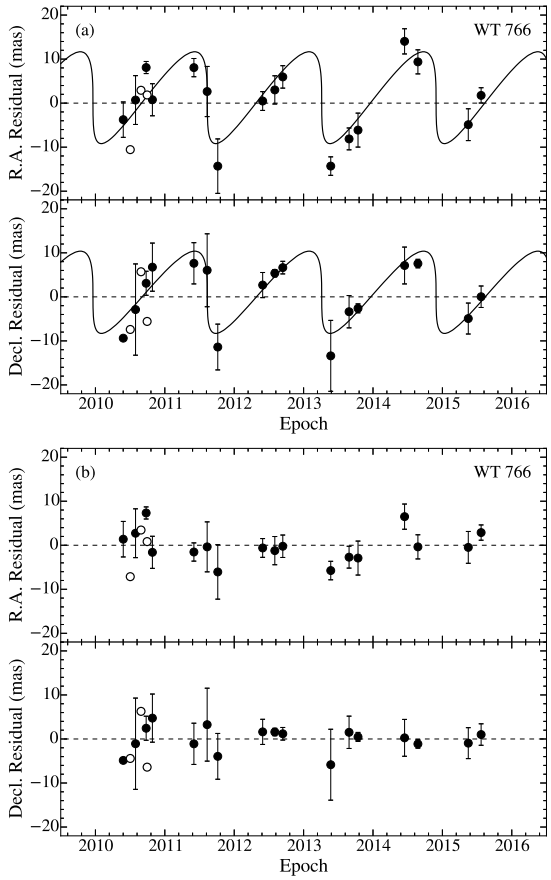

Fig. 10.— Nightly mean astrometric residual plots for WT 766, a common proper motion companion to WD 2057−493. The upper panel (*a*) shows the raw residuals and the best-fit orbital solution while the lower panel (*b*) shows the residuals once the orbital solution is applied. In both plots, the open circles represent data for which only one frame was taken on that night. The astrometric solution presented in Table 2 for WT 766 accounts for the orbital solution.

munication) as a blue companion to a *Hipparcos* star within 25 pc. We note that the recent work of Holberg et al. (2016) has also identified this object as a WD based on its colors but does not have a spectrum and instead assumes it to be a DA WD. We obtained an identification spectrum with the SOAR + Goodman spectrograph as described in Section 2.2. The spectrum, shown in Figure 1, indicates the object is a relatively cool DB WD and its companion distance via *Hipparcos* & TGAS of 21.1 ± 0.1 pc is adopted for this WD making it a new member of the 25 pc WD sample.

WD 2326+049, better known as G29−38, is a variable ZZ Ceti WD (Shulov & Kopatskaya 1974) with significant IR excess (Zuckerman & Becklin 1987) and one of the first WDs found with metal pollution (Koester et al. 1997). Thus, the spectral classification is DAZV. The previous trigonometric parallax from YPC of 73.4 ± 4.0 mas is significantly larger than our measure of 56.83 ± 0.39 mas. This distance discrepancy will have an impact on the implied surface gravity and, thus, on settling times for the accreted metals. The abundance analysis performed by Xu et al. (2014) notes that the implied surface gravity of 8.4 dex from the previous parallax measurement produced inconsistent model spectroscopic line profiles from those observed, suggesting that a lower surface gravity is likely. Indeed, our updated parallax suggests a log g = 8.00 ± 0.03. Because the IR excess affects the near-IR HK_s photometry, these measures have been excluded from the model fit.

5. Discussion

5.1. 25 pc White Dwarf Sample

Prior to the CTIOPI effort to obtain a volume-limited sample of WDs within 25 pc, whose first WD results were published in 2009 (Subasavage et al. 2009), a total of 112 systems, of which 99 had robust trigonometric parallax determinations (i.e., better than 10%), were known. The contributions to the 25 pc sample, both prior to 2009 and since, are tabulated in Table 6. Prior to this work, the 25 pc WD sample consisted of 137 systems, of which 126 systems have robust trigonometric parallax determinations. The trigonometric parallaxes presented in this work consist of 23 new systems from CTIOPI, 19 new systems from NOFS, one new system measured by both programs, as well as seven of the eleven systems with poor previous trigonometric parallax determinations, i.e., worse than 10%. Two additional systems, one new (WD 0148+641) and one with a poor previous parallax determination (WD 2117+539), have parallax determinations from NOFS and are also included in the recently published TGAS catalog with measurements confirming 25 pc sample membership. Finally, we spectroscopically confirm that WD 2307−691 is a WD companion to

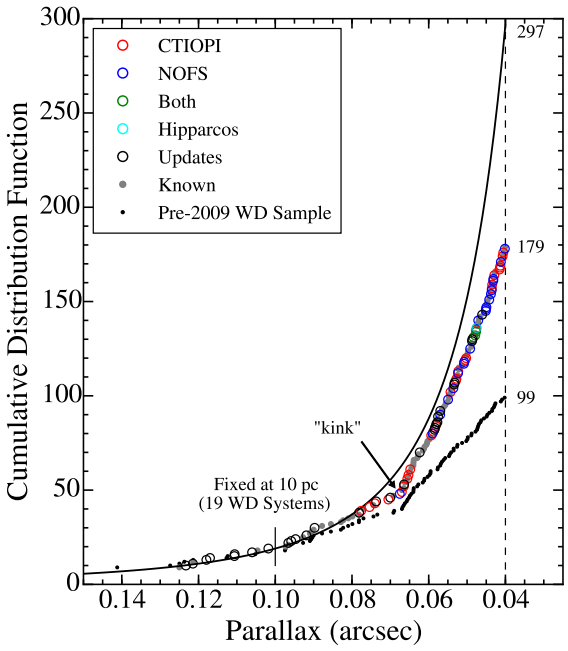

Fig. 11.— Cumulative distribution plot for the 25 pc WD sample. New additions presented in this work are highlighted by sub-sample as shown in the legend. The black points represent the 25 pc WD sample prior to 2009 and serve as an indicator of the progress made since. The numbers to the right of the curves (99, 179 and 297) represent the number of systems at 25 pc prior to 2009, now, and that expected at 25 pc, respectively, indicating ∼40% incompleteness currently. The "kink" described in Section 5.1 is identified with an arrow.

HIP 114416, with a *Hipparcos*+TGAS trigonometric parallax distance of 21.0 ± 0.1 pc. The final number of members added by this work is 53 systems, thereby increasing the sample completeness by 42% to 179 systems. The measured local WD density is then 2.7 × 10^{-3} pc^{-3} based on this sample. This value is considerably lower than that found by Holberg et al. (2016) of 4.8 × 10^{-3} pc^{-3}, because those authors include the expected incompleteness based on a complete 13 pc sample. As shown in Figure 11, assuming a constant density and that all WD systems within 10 pc are known, we expect this sample to be incomplete at the ∼40% level even after the addition of the new members presented here. Accounting for this expected incompleteness, we arrive at an expected local WD density of 4.5 × 10^{-3} pc^{-3}, very similar to that found by Holberg et al. (2016). Another curiosity seen in the figure is the "kink" in observed systems around 15 pc, thus implying a dearth of WD systems at that distance. While a few new systems were found at and within that distance, pure incompleteness from single field WDs is not likely a significant factor. There is the possibility that new WD systems will be identified as companions to bright main-sequence primaries (the so-called "Sirius-like" systems) that may reduce the dearth.

Gaia is a cornerstone mission in the science programme of the European Space Agency (ESA) that will deliver unprecedented astrometric accuracy for one billion stars in the Milky Way. A description of the mission is given by Gaia Collaboration et al. (2016b). While *Gaia* will effectively complete the 25 pc WD sample and beyond (Silvotti et al. 2015, estimates effective WD completeness by *Gaia* out to ∼55 pc), the DR1 released in 2016 (Gaia Collaboration et al. 2016a) only includes trigonometric parallaxes for *Hipparcos* and *Tycho* stars and thus, did not contain new sample members beyond the two mentioned above.

5.2. Sky Distribution

Traditionally, the southern hemisphere has been undersampled relative to the north simply because there are more observing assets in the north. In particular, as nearby stars tend to be identified via proper motion surveys, it is only recently that proper motion surveys in the south (e.g., Lépine & Shara 2005; Boyd et al. 2011) have pushed to sufficiently low proper motions to better identify nearby, slow movers. With the samples presented here, we have effectively removed the bias towards northern targets (see Table 7) as there are now almost identical numbers, 90 and 89 in the northern and southern hemispheres, respectively. An Aitoff projection of the 25 pc WD sky distribution is shown in Figure 12.

6. Conclusions

With respect to individual systems presented here, we find four that are very strong halo candidates (WD 1237−230, $V_{\rm tan} = 202.4$ km sec^{-1}; WD 1314−153, $V_{\rm tan} = 191.7$ km sec^{-1}; WD 1339−340, $V_{\rm tan} = 255.0$ km sec^{-1}; and WD 2226−754AB,

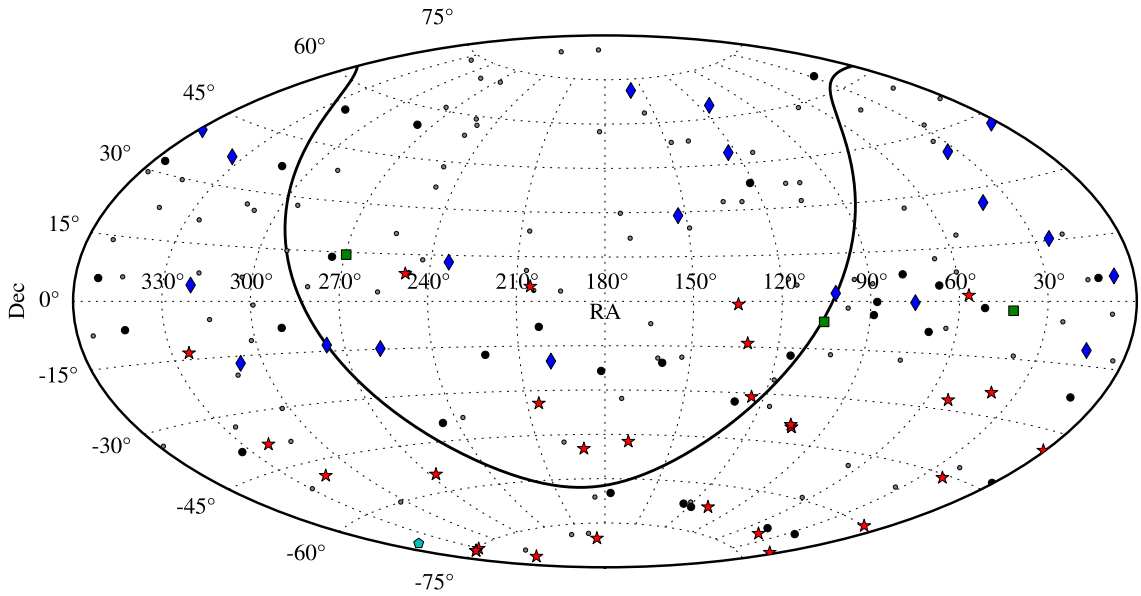

Fig. 12.— Aitoff projection of the 25 pc WD sample. The curve represents the Galactic Plane. Previously known WD systems (*small gray circles*) and updates (*large filled circles*) are shown. New additions from CTIOPI (*red stars*), NOFS (*blue diamonds*), both programs (*green squares*), as well as the lone *Hipparcos* companion (*cyan pentagon*) are also shown. Note that the two systems measured by the *Gaia* TGAS survey are included in the NOFS sample for which parallaxes were confirmed.

$V_{\rm tan} = 135.3$ km sec^{-1}) based on kinematics alone and they often have other supporting evidence collected by other researchers. Two of these systems are mere interlopers that happen to be within the 25 pc volume at present (WD 1339−340 and WD 2226−754AB). As discussed in Section 4.2, WD 1237−230 is an unresolved double degenerate so our mass estimate is incorrect. For the three other halo candidates, the masses are entirely consistent with old total ages, i.e., when the main-sequence progenitor lifetimes are taken into account (see Bergeron et al. 2005, their Figure 9) expected for halo membership.

We find two very cool WDs that display CIA such that they appear relatively blue (WD 0222−291 and WD 0851−246). Additionally, near-IR photometry collected during this effort shows WD 0851−246 to have excess in JHK_S suggesting a red unseen companion to the WD which is, itself, a common proper motion companion to a widely separated cool, old subdwarf.

We spectroscopically identify a metal-rich DAZ WD (WD 2028−171) and confirm it to be within the 25 pc volume. Follow-up observations will enable a thorough analysis of this remnant planetary system signature.

Our sample contains at least three systems that appear overluminous (WD 1237−230, WD 1242−105, and WD 1447−190) and, thus, are likely unresolved multiples. We conducted follow-up spectroscopic observations for two (WD 1242−105 and WD 1447−190) and find that WD 1242−105 is a short-period double degenerate, confirming the independent work of Debes et al. (2015), and that WD 1447−190 is a single-lined spectroscopic binary with a radial velocity variation over a few days, but have not constrained the orbit. Radial velocity work by Kawka & Vennes (2012) confirms that WD 1237−230 is a single-lined binary. Two WDs are marginally overluminous (WD 0233−242 and WD 1817−598); however, they are both spectroscopically featureless DC WDs that prohibit radial velocity analyses for confirmation. We see no astrometric perturbations for either of these two systems.

Two of our objects do show astrometric pertur-

bations. WD 1814+134 shows a long-period residual that has gone unrecognized in short baseline astrometric datasets but is visible from the ∼13-year baseline of the CTIOPI astrometric data. WD 2057−493 is a newly identified nearby WD that we spectroscopically identified in this work and has a main-sequence common proper motion companion (likely an early M-dwarf though no spectral confirmation was acquired). Astrometric data were collected on both members of the system and the main-sequence star shows a clear astrometric perturbation with a period of 1.648 years. The astrometric dataset encompasses ∼3 full periods and, given that the astrometric solution for the WD companion used an identical reference field and shows flat residuals, the perturbation detection is robust.

Of the 107 systems whose trigonometric parallaxes are presented here, 50 are new members of the 25 pc WD sample. In addition, two systems (WD 0148+641 and WD 2117+539) have recently determined trigonometric parallaxes from the TGAS catalog with which our trigonometric parallaxes agree and confirm sample membership. Finally, we spectroscopically confirmed a newly identified WD companion (WD 2307−691) to *Hipparcos* star HIP 114416 with a trigonometric parallax within 25 pc that we adopt for the WD companion. Thus, a total of 53 new 25 pc WD systems have been added to a sample of 126 prior systems with robust distance determinations resulting in a 42% increase. Between the CTIOPI and NOFS parallax programs overall, a total of 70 new WD systems have been added to the 25 pc WD sample – a 64% increase to the sample. It is expected that *Gaia* will largely complete this sample upon release of its final catalog (if not in one of the early data releases), save for, perhaps, in regions near the Galactic plane where crowding will cause greater incompleteness. This 25 pc sample represents the pre-*Gaia* collection of knowledge for the sample and will serve to clearly demonstrate the (most likely) significant contribution that *Gaia* will make in this arena.

We would like to thank the referee for a number of comments and suggestions that have clarified several points. We thank the members of the SMARTS Consortium, who enable the operations of the small telescopes at CTIO, as well as the observer support at CTIO, specifically Edgardo Cosgrove, Arturo Gomez, Alberto Miranda, and Joselino Vasquez. We thank Nicole van der Bliek, Andrea Kunder, and Ron Probst for their assistance with the NEWFIRM dataset. We thank the observer support at NOFS, specifically Michael DiVittorio, Fred Harris, Albert Rhodes, and Michael Schultheis. Additionally, we thank the individuals that have assisted with the NOFS parallax program's observations over the many years of operation, including Blaise Canzian, Harry Guetter, Stephen Levine, Christian Luginbuhl, Jeff Munn, and Trudy Tilleman.

The RECONS team wishes to thank the NSF (grants AST 05−07711, AST 09−08402, and AST 14−12026) and GSU for their continued support in our study of nearby stars. P. B. and P. D. wish to acknowledge the support of NSERC Canada as well as the the Fund FRQNT (Québec).

Based on observations (GS-2012A-Q-36) obtained at the Gemini Observatory, acquired through the Gemini Science Archive and processed using the Gemini IRAF package, which is operated by the Association of Universities for Research in Astronomy, Inc., under a cooperative agreement with the NSF on behalf of the Gemini partnership: the National Science Foundation (United States), the National Research Council (Canada), CONICYT (Chile), Ministerio de Ciencia, Tecnología e Innovación Productiva (Argentina), and Ministério da Ciência, Tecnologia e Inovação (Brazil).

Based on observations obtained at the Southern Astrophysical Research (SOAR) telescope, which is a joint project of the Ministério da Ciência, Tecnologia, e Inovação (MCTI) da República Federativa do Brasil, the U.S. National Optical Astronomy Observatory (NOAO), the University of North Carolina at Chapel Hill (UNC), and Michigan State University (MSU).

This publication makes use of data products from the Two Micron All Sky Survey, which is a joint project of the University of Massachusetts and the Infrared Processing and Analysis Center/California Institute of Technology, funded by the National Aeronautics and Space Administration and the National Science Foundation.

This work has made use of data from the European Space Agency (ESA) mission *Gaia* (`http://www.cosmos.esa.int/gaia`), processed

by the *Gaia* Data Processing and Analysis Consortium (DPAC, `http://www.cosmos.esa.int/web/gaia/dpac/consortium`). Funding for the DPAC has been provided by national institutions, in particular the institutions participating in the *Gaia* Multilateral Agreement.

Funding for SDSS-III has been provided by the Alfred P. Sloan Foundation, the Participating Institutions, the National Science Foundation, and the U.S. Department of Energy Office of Science. The SDSS-III web site is http://www.sdss3.org/.

SDSS-III is managed by the Astrophysical Research Consortium for the Participating Institutions of the SDSS-III Collaboration including the University of Arizona, the Brazilian Participation Group, Brookhaven National Laboratory, University of Cambridge, Carnegie Mellon University, University of Florida, the French Participation Group, the German Participation Group, Harvard University, the Instituto de Astrofisica de Canarias, the Michigan State/Notre Dame/JINA Participation Group, Johns Hopkins University, Lawrence Berkeley National Laboratory, Max Planck Institute for Astrophysics, Max Planck Institute for Extraterrestrial Physics, New Mexico State University, New York University, Ohio State University, Pennsylvania State University, University of Portsmouth, Princeton University, the Spanish Participation Group, University of Tokyo, University of Utah, Vanderbilt University, University of Virginia, University of Washington, and Yale University.

REFERENCES

Alam, S., Albareti, F. D., Allende Prieto, C., et al. 2015, ApJS, 219, 12

Aznar Cuadrado, R., Jordan, S., Napiwotzki, R., et al. 2004, A&A, 423, 1081

Bergeron, P., Ruiz, M. T., & Leggett, S. K. 1997, ApJS, 108, 339

Bergeron, P. 2003, ApJ, 586, 201

Bergeron, P., Ruiz, M. T., Hamuy, M., et al. 2005, ApJ, 625, 838

Bergeron, P., Saumon, D., & Wesemael, F. 1995, ApJ, 443, 764

Bertin, E. 2011, Astronomical Data Analysis Software and Systems XX, 442, 435

Bertin, E., & Arnouts, S. 1996, A&AS, 117, 393

Boyd, M. R., Henry, T. J., Jao, W.-C., Subasavage, J. P., & Hambly, N. C. 2011, AJ, 142, 92

Carpenter, J. M. 2001, AJ, 121, 2851

Casali, M., Adamson, A., Alves de Oliveira, C., et al. 2007, A&A, 467, 777

Chauvin, G., Lagrange, A.-M., Udry, S., Fusco, T., Galland, F., Naef, D., Beuzit, J.-L., & Mayor, M. 2006, A&A, 456, 1165

Dahn, C. C., Harris, H. C., Vrba, F. J., et al. 2002, AJ, 124, 1170

Debes, J. H., & Kilic, M. 2010, American Institute of Physics Conference Series, 1273, 488

Debes, J. H., Kilic, M., Tremblay, P.-E., et al. 2015, AJ, 149, 176

Ducourant, C., Teixeira, R., Hambly, N. C., Oppenheimer, B. R., Hawkins, M. R. S., Rapaport, M., Modolo, J., & Lecampion, J. F. 2007, A&A, 470, 387

Dufour, P., Bergeron, P., & Fontaine, G. 2005, ApJ, 627, 404

Dufour, P., Bergeron, P., Liebert, J., et al. 2007, ApJ, 663, 1291

Farihi, J., Dufour, P., Napiwotzki, R., & Koester, D. 2011, MNRAS, 413, 2559

Farihi, J., Jura, M., & Zuckerman, B. 2009, ApJ, 694, 805

Fontaine, G., Brassard, P., & Bergeron, P. 2001, PASP, 113, 409

Gaia Collaboration, Brown, A. G. A., Vallenari, A., et al. 2016a, A&A, 595, A2

Gaia Collaboration, Prusti, T., de Bruijne, J. H. J., et al. 2016b, A&A, 595, A1

Gatewood, G., & Coban, L. 2009, AJ, 137, 402

Giammichele, N., Bergeron, P., & Dufour, P. 2012, ApJS, 199, 29

Gianninas, A., Bergeron, P., & Ruiz, M. T. 2011, ApJ, 743, 138

Gianninas, A., Curd, B., Thorstensen, J. R., et al. 2015, MNRAS, 449, 3966

Gould, A., & Chanamé, J. 2004, ApJS, 150, 455

Graham, J. A. 1982, PASP, 94, 244

Hambly, N. C., Collins, R. S., Cross, N. J. G., et al. 2008, MNRAS, 384, 637

Hansen, B. M. S. 1998, Nature, 394, 860

Harris, H. C., Dahn, C. C., Zacharias, N., et al. 2016, AJ, 152, 118

Henry, T. J., Subasavage, J. P., Brown, M. A., Beaulieu, T. D., Jao, W., & Hambly, N. C. 2004, AJ, 128, 2460

Hewett, P. C., Warren, S. J., Leggett, S. K., & Hodgkin, S. T. 2006, MNRAS, 367, 454

Hodgkin, S. T., Irwin, M. J., Hewett, P. C., & Warren, S. J. 2009, MNRAS, 394, 675

Holberg, J. B., & Bergeron, P. 2006, AJ, 132, 1223

Holberg, J. B., Oswalt, T. D., Sion, E. M., & McCook, G. P. 2016, MNRAS, 462, 2295

Jao, W.-C., Henry, T. J., Subasavage, J. P., Brown, M. A., Ianna, P. A., Bartlett, J. L., Costa, E., & Méndez, R. A. 2005, AJ, 129, 1954

Jefferys, W. H., Fitzpatrick, M. J., & McArthur, B. E. 1988, Celestial Mechanics, 41, 39

Kawka, A., & Vennes, S. 2006, ApJ, 643, 402

Kawka, A., & Vennes, S. 2012, MNRAS, 425, 1394

Kawka, A., Vennes, S., Schmidt, G. D., Wickramasinghe, D. T., & Koch, R. 2007, ApJ, 654, 499

Kawka, A., Vennes, S., & Thorstensen, J. R. 2004, AJ, 127, 1702

Kilic, M., Kowalski, P. M., Reach, W. T., & von Hippel, T. 2009, ApJ, 696, 2094

Kilkenny, D., Heber, U., & Drilling, J. S. 1988, South African Astronomical Observatory Circular, 12,

Kirkpatrick, J. D., Henry, T. J., & Simons, D. A. 1995, AJ, 109, 797

Koerner, D. W., Henry, T. J., Fuhrman, L. A., et al. 2003, Bulletin of the American Astronomical Society, 35, 42.07

Koester, D., Provencal, J., & Shipman, H. L. 1997, A&A, 320, L57

Koester, D., Rollenhagen, K., Napiwotzki, R., et al. 2005, A&A, 432, 1025

Koester, D., Girven, J., Gänsicke, B. T., & Dufour, P. 2011, A&A, 530, A114

Landolt, A. U. 1992, AJ, 104, 340

Landolt, A. U. 2007, AJ, 133, 2502

Landolt, A. U. 2013, AJ, 146, 131

Lawrence, A., Warren, S. J., Almaini, O., et al. 2007, MNRAS, 379, 1599

Lépine, S., Rich, R. M., & Shara, M. M. 2003, AJ, 125, 1598

Lépine, S., Rich, R. M., & Shara, M. M. 2005, ApJ, 633, L121

Lépine, S., & Shara, M. M. 2005, Bulletin of the American Astronomical Society, 37, 150.01

Lépine, S., Shara, M. M., & Rich, R. M. 2002, AJ, 124, 1190

Lépine, S., Thorstensen, J. R., Shara, M. M., & Rich, R. M. 2009, AJ, 137, 4109

Liebert, J., & Strittmatter, P. A. 1977, ApJ, 217, L59

Limoges, M.-M., Bergeron, P., & Lépine, S. 2015, ApJS, 219, 19

Lindegren, L., Lammers, U., Bastian, U., et al. 2016, A&A, 595, A4

Luyten, W. J. 1972, Proper Motion Survey, University of Minnesota, 30,

Luyten, W. J., & La Bonte, A. E. 1972, Proper Motion Survey, University of Minnesota, 32,

Luyten, W. J. 1974, Proper Motion Survey, University of Minnesota, 37,

Luyten, W. J. 1979a, New Luyten catalogue of stars with proper motions larger than two tenths of an arcsecond; and first supplement; NLTT. (Minneapolis (1979)); Label 12 = short description; Label 13 = documentation by Warren; Label 14 = catalogue, Strasbourg version,

Luyten, W. J. 1979b, Minneapolis: University of Minnesota, 1979, 2nd ed., LHS

McGraw, J. T., & Robinson, E. L. 1975, ApJ, 200, L89

Monet, D. G., & Dahn, C. C. 1983, AJ, 88, 1489

Monet, D. G., Dahn, C. C., Vrba, F. J., et al. 1992, AJ, 103, 638

Mugrauer, M., & Neuhäuser, R. 2005, MNRAS, 361, L15

Oppenheimer, B. R., Hambly, N. C., Digby, A. P., Hodgkin, S. T., & Saumon, D. 2001, Science, 292, 698

Press, W. H., Teukolsky, S. A., Vetterling, W. T., & Flannery, B. P. 1992, Numerical Recipes in FORTRAN, 2nd edition (Cambridge: Cambridge University Press), 644

Probst, R. G., Gaughan, N., Abraham, M., et al. 2004, Proc. SPIE, 5492, 1716

Reimers, D., Jordan, S., Koester, D., et al. 1996, A&A, 311, 572

Ruiz, M. T., & Bergeron, P. 2001, ApJ, 558, 761

Ruiz, M. T., Wischnjewsky, M., Rojo, P. M., & Gonzalez, L. E. 2001, ApJS, 133, 119

Salim, S., Rich, R. M., Hansen, B. M., et al. 2004, ApJ, 601, 1075

Saumon, D., Bergeron, P., Lunine, J. I., Hubbard, W. B., & Burrows, A. 1994, ApJ, 424, 333

Saumon, D., & Jacobson, S. B. 1999, ApJ, 511, L107

Sayres, C., Subasavage, J. P., Bergeron, P., et al. 2012, AJ, 143, 103

Schlafly, E. F., & Finkbeiner, D. P. 2011, ApJ, 737, 103

Schmidt, G. D., Vennes, S., Wickramasinghe, D. T., & Ferrario, L. 2001, MNRAS, 328, 203

Scholz, R.-D., Szokoly, G. P., Andersen, M., Ibata, R., & Irwin, M. J. 2002, ApJ, 565, 539

Silvestri, N. M., Oswalt, T. D., & Hawley, S. L. 2002, AJ, 124, 1118

Silvotti, R., Sozzetti, A., Lattanzi, M., & Morbidelli, R. 2015, 19th European Workshop on White Dwarfs, 493, 455

Sion, E. M., Greenstein, J. L., Landstreet, J. D., et al. 1983, ApJ, 269, 253

Shulov, O. S., & Kopatskaya, E. N. 1974, *Astrofizika*, 10, 117

Smart, R. L., et al. 2003, A&A, 404, 317

Stetson, P. B. 1987, PASP, 99, 191

Strand, K. A. 1964, S&T, 27,

Subasavage, J. P., Henry, T. J., Bergeron, P., et al. 2007, AJ, 134, 252

Subasavage, J. P., Henry, T. J., Bergeron, P., Dufour, P., & Hambly, N. C. 2008, AJ, 136, 899

Subasavage, J. P., Jao, W.-C., Henry, T. J., et al. 2009, AJ, 137, 4547

Tremblay, P.-E., & Bergeron, P. 2009, ApJ, 696, 1755

Vennes, S., & Kawka, A. 2003, ApJ, 586, L95

van Altena, W. F., Lee, J. T., & Hoffleit, E. D. 1995, New Haven, CT: Yale University Observatory, —c1995, 4th ed., completely revised and enlarged

van Leeuwen, F. 2007, Hipparcos, the New Reduction of the Raw Data. By Floor van Leeuwen, Institute of Astronomy, Cambridge University, Cambridge, UK Series: Astrophysics and Space Science Library, Vol. 350 20 Springer Dordrecht

Xu, S., Jura, M., Koester, D., Klein, B., & Zuckerman, B. 2014, ApJ, 783, 79

Zuckerman, B., & Becklin, E. E. 1987, Nature, 330, 138

Zuckerman, B., Koester, D., Reid, I. N., Hünsch, M. 2003, ApJ, 596, 477

This 2-column preprint was prepared with the AAS LaTeX macros v5.2.

Table 1
Photometric Results

Name (1)	Alternate Name (2)	B_J (3)	N_B (4)	V_J (5)	N_V (6)	R_{KC} (7)	N_R (8)	I_{KC} (9)	N_I (10)	π Filter (11)	σ (mag) (12)	No. of Nights (13)	No. of Frames (14)	J_{2M} (15)	H_{2M} (16)	$K_{S_{2M}}$ (17)	Notes (18)
WD2359−434	LHS 1005	···	···	12.97	3	12.82	3	12.66	3	R	0.007	23	142	12.60± 0.03	12.43± 0.02	12.45± 0.02	a
WD0000−345	LHS 1008	15.42	2	15.03	4	14.73	4	14.43	4	R	0.007	14	61	14.12± 0.02	14.02± 0.04	13.92± 0.06	
WD0008+424	GD 5	···	···	···	···	···	···	···	···	···	···	···	···	14.54± 0.03	14.35± 0.04	14.39± 0.06	
WD0011−721	LP 50−73	···	···	15.17	3	14.87	3	14.55	3	R	0.006	13	66	14.21± 0.03	13.97± 0.04	13.91± 0.05	b
WD0025+054	LSPM J0027+0542	16.79	1	16.15	1	15.76	1	15.38	1	···	···	···	···	14.92± 0.02	14.65± 0.02	14.56± 0.02	c
WD0034−602	LP 122−4	14.19	2	14.08	3	14.19	3	14.20	3	R	0.006	14	59	14.37± 0.04	14.55± 0.06	14.52± 0.09	d
WD0038−226	GJ 2012	15.15	2	14.49	5	14.08	4	13.67	5	R	0.006	29	133	13.34± 0.03	13.48± 0.03	13.74± 0.04	e
WD0046+051	LHS 7	12.91	2	12.38	3	12.15	3	11.89	3	R	0.006	15	77	11.69± 0.02	11.57± 0.02	11.50± 0.03	
WD0053−117	LP 706−65	15.62	3	15.25	3	···	···	14.77	3	···	···	···	···	14.51± 0.03	14.35± 0.04	14.29± 0.07	
WD0123−460	SCR 0125−4545	···	···	16.30	3	15.94	3	15.57	3	R	0.007	15	63	15.11± 0.04	14.84± 0.06	14.91± 0.10	b
WD0127−311	GJ 2023	···	···	15.74	2	15.70	2	15.66	2	V	0.007	15	59	15.73± 0.07	15.91± 0.20	15.68± Null	
WD0136+152	PG 0136+152	15.19	2	14.94	2	···	···	14.60	2	···	···	···	···	14.41± 0.02	14.29± 0.02	14.27± 0.02	c
WD0141−675	LHS 145	···	···	13.82	3	13.52	3	13.23	3	V	0.006	31	163	12.87± 0.02	12.66± 0.03	12.58± 0.03	a
WD0148+641	G244−36	14.20	1	13.98	1	13.84	1	13.67	1	···	···	···	···	··· ± ···	··· ± ···	··· ± ···	
WD0150+256	G94−21	···	···	15.71	3	15.52	3	15.32	3	R	0.007	13	54	15.07± 0.04	15.07± 0.09	15.15± 0.14	f
WD0213+396	GD 25	14.78	1	14.58	2	···	···	14.33	2	···	···	···	···	14.30± 0.03	14.22± 0.05	14.14± 0.05	
WD0222−291	LHS 1402	···	···	18.05	3	18.00	3	18.34	3	R	0.015	22	44	··· ± ···	··· ± ···	··· ± ···	g
WD0226−329	LP 941−91	13.77	2	13.86	4	13.97	4	14.08	4	R	0.006	13	53	14.41± 0.03	14.47± 0.05	14.70± 0.09	
WD0233−242	LHS 1421	···	···	15.94	3	15.43	3	14.93	3	R	0.006	14	62	14.45± 0.03	14.34± 0.05	14.12± 0.07	b
WD0236+259	G36−29	···	···	···	···	···	···	···	···	···	···	···	···	14.91± 0.03	14.61± 0.05	14.47± 0.07	
WD0243−026	LHS 1442	15.90	3	15.53	4	15.27	3	14.99	4	R	0.007	11	57	14.68± 0.04	14.59± 0.04	14.48± 0.09	
WD0255−705	LHS 1474	···	···	14.07	4	14.04	4	13.99	4	R	0.007	13	62	14.04± 0.03	14.12± 0.04	13.99± 0.06	f
WD0310−688	GJ 127.1A	···	···	11.38	3	11.47	3	11.55	3	R	0.008	16	74	11.76± 0.02	11.79± 0.03	11.86± 0.02	
WD0311−649	WT 106	···	···	13.28	3	13.33	3	13.36	3	R	0.004	15	69	13.45± 0.02	13.46± 0.03	13.57± 0.05	h
WD0322−019	G77−50	16.94	2	16.13	2	···	···	15.27	2	···	···	···	···	14.76± 0.04	14.44± 0.05	14.38± 0.08	
···	LHS 1550	···	···	13.75:	2	12.58:	2	11.07:	2	R	[0.014]	11	57	9.60± 0.03	9.00± 0.02	8.77± 0.02	i,j
WD0326−273	LHS 1549	···	···	13.61:	2	13.50:	2	13.42:	2	R	[0.011]	11	57	13.22± 0.10	13.11± 0.09	13.10± 0.12	i,j
WD0344+014	LHS 5084	···	···	16.51	3	16.02	3	15.54	3	R	0.007	12	61	15.00± 0.04	14.87± 0.10	14.70± 0.12	f
WD0423+044	LHS 1670	18.14	1	17.14	1	···	···	16.11	1	···	···	···	···	15.47± 0.07	15.18± 0.08	15.17± 0.15	
WD0435−088	LHS 194	···	···	13.75	3	13.44	3	13.18	3	R	0.009	25	137	13.01± 0.03	12.91± 0.03	12.76± 0.04	
WD0457−004	G84−26	···	···	···	···	···	···	···	···	···	···	···	···	15.33± 0.05	15.20± 0.09	15.36± 0.17	
WD0511+079	G84−41	16.30	2	15.87	2	···	···	15.33	2	···	···	···	···	15.11± 0.05	14.92± 0.06	14.86± 0.08	
WD0548−001	GJ 1086	15.06	2	14.60	4	14.21	4	13.96	4	R	0.008	20	93	13.73± 0.03	13.68± 0.03	13.71± 0.04	
WD0552−041	GJ 223.2	···	···	14.47	3	13.99	3	13.51	3	R	0.007	38	235	13.05± 0.03	12.86± 0.03	12.78± 0.03	a
WD0644+025	G108−26	16.02	2	15.67	2	15.46	2	15.18	2	···	···	···	···	14.97± 0.02	14.81± 0.02	14.77± 0.02	c
WD0651−398B	WT 201	···	···	16.07	3	15.75	3	15.45	3	R	0.007	12	52	15.10± 0.05	14.90± 0.08	14.71± 0.12	h
WD0651−398A	WT 202	···	···	15.46	3	15.23	3	14.98	3	R	0.006	12	52	14.71± 0.04	14.55± 0.05	14.49± 0.11	h
WD0655−390	GJ 2054	···	···	15.11	3	14.81	3	14.48	3	R	0.007	11	48	14.15± 0.03	13.88± 0.04	13.89± 0.07	b
WD0659−063	LHS 1892	···	···	15.44	3	15.15	3	14.86	3	R	0.007	11	57	14.55± 0.03	14.35± 0.03	14.29± 0.03	c
WD0708−670	SCR 0708−6706	···	···	16.22	3	15.72	3	15.21	3	R	0.005	13	59	14.71± 0.03	14.65± 0.05	14.47± 0.07	b
WD0728+642	G234−4	17.07	2	16.22	2	···	···	15.32	2	···	···	···	···	14.81± 0.03	14.52± 0.04	14.39± 0.07	
···	GJ 283B	···	···	16.69	4	14.69	4	12.41	4	I	0.009	29	165	10.15± 0.02	9.63± 0.02	9.29± 0.02	a
WD0738−172	GJ 283A	···	···	13.06	4	12.89	4	12.72	4	I	0.006	29	165	12.65± 0.02	12.61± 0.03	12.58± 0.04	a
WD0752−676	GJ 293	···	···	13.96	3	13.58	3	13.20	3	R	0.007	26	144	12.73± 0.02	12.48± 0.03	12.36± 0.02	a
WD0802+387	LHS 1980	17.88	2	16.89	2	···	···	15.97	2	···	···	···	···	15.34± 0.05	15.19± 0.08	14.90± 0.09	
WD0810+489	G111−64	51.45	2	15.07	2	14.81	2	14.56	2	···	···	···	···	14.32± 0.03	14.13± 0.04	14.06± 0.06	
WD0816−310	SCR 0818−3110	···	···	15.43	3	15.21	3	15.05	3	R	0.008	11	49	14.92± 0.04	14.73± 0.07	14.83± 0.12	b
WD0821−669	SCR 0821−6703	···	···	15.34	3	14.82	3	14.32	3	R	0.006	36	184	13.79± 0.03	13.57± 0.03	13.34± 0.04	d
WD0839−327	GJ 318	···	···	11.86	3	11.77	3	11.65	3	V	0.006	15	91	11.58± 0.03	11.54± 0.03	11.55± 0.03	a
WD0840−136	LP 726−1	···	···	15.72	3	15.36	3	15.02	3	R	0.006	17	78	14.62± 0.03	14.41± 0.05	14.54± 0.09	d
···	LHS 2067	···	···	17.94	3	16.29	3	14.20	3	I	0.006	22	71	12.39± 0.02	11.88± 0.02	11.57± 0.02	
WD0851−246	LHS 2068	···	···	18.09	3	17.56	3	17.47	3	I	0.018	22	71	*17.10± 0.04*	*16.55± 0.08*	*16.20± 0.08*	g,k
WD0856−007	LP 606−32	···	···	16.33	3	15.85	3	15.39	3	R	0.013	16	68	14.83± 0.04	14.58± 0.05	14.69± 0.13	b,f
WD1008+290	LHS 2229	18.19	3	17.51	4	16.11	2	15.59	4	···	···	···	···	15.13± 0.05	14.72± 0.06	14.54± 0.08	
WD1016−308	LP 904−3	14.75	1	14.68	4	14.76	4	14.82	4	R	0.008	11	51	15.05± 0.04	15.12± 0.08	15.41± 0.21	f
WD1033+714	LHS 285	17.97	2	16.94	2	···	···	15.87	2	···	···	···	···	15.19± 0.05	14.84± 0.08	14.98± 0.15	
WD1036−204	LHS 2293	16.37	1	16.25	4	15.54	3	15.33	4	R	0.006	28	117	14.63± 0.03	14.35± 0.04	14.04± 0.07	f
WD1105−340	SCR 1107−3420A	···	···	13.66	3	13.73	3	13.78	3	R	0.007	20	93	13.95± 0.03	13.98± 0.04	14.05± 0.07	f
···	SCR 1107−3420B	···	···	15.04	3	13.68	3	11.96	3	R	0.016	20	93	10.26± 0.02	9.70± 0.02	9.41± 0.02	g
WD1116−470	SCR 1118−4721	···	···	15.52	3	15.20	3	14.86	3	R	0.007	11	47	14.45± 0.03	14.37± 0.06	14.35± 0.09	b
WD1124−293	ESO 439−80	15.23	1	15.04	3	14.93	4	14.81	4	R	0.006	12	60	14.78± 0.03	14.71± 0.04	14.60± 0.09	
WD1142−645	GJ 440	···	···	11.50	3	11.34	3	11.20	3	V	0.007	35	214	11.19± 0.02	11.13± 0.03	11.10± 0.03	a
WD1149−272	LEHPM 2−4051	···	···	15.87	4	15.59	4	15.37	4	R	0.008	25	102	15.17± 0.05	14.92± 0.07	14.77± 0.11	d

TABLE 1—*Continued*

Name (1)	Alternate Name (2)	B_J (3)	N_B (4)	V_J (5)	N_V (6)	R_{KC} (7)	N_R (8)	I_{KC} (9)	N_I (10)	π Filter (11)	σ (mag) (12)	No. of Nights (13)	No. of Frames (14)	J_{2M} (15)	H_{2M} (16)	$K_{S_{2M}}$ (17)	Notes (18)
WD1202−232	LP 852−7	···	···	12.80	3	12.66	3	12.52	3	R	0.006	27	132	12.40± 0.02	12.30± 0.03	12.34± 0.03	d
WD1236−495	LHS 2594	13.97	1	13.81	3	13.81	3	13.78	3	R	0.005	13	63	13.81± 0.02	13.81± 0.04	13.91± 0.06	
WD1237−230	LHS 339	17.16	1	16.54	3	16.13	3	15.72	3	R	0.008	10	47	15.35± 0.05	15.08± 0.08	14.94± 0.11	f
WD1242−105	LP 736−4	···	···	14.73	3	14.57	3	14.38	3	V	0.006	14	63	14.23± 0.03	14.07± 0.03	14.08± 0.06	
WD1241−798	LHS 2621	···	···	16.18	3	15.80	3	15.45	3	V	0.006	9	44	15.03± 0.05	14.83± 0.07	14.60± 0.12	b
WD1313−198	LHS 2710	17.94	2	17.16	2	···	···	16.32	2	···	···	···	···	15.88± 0.08	15.61± 0.10	15.55± 0.19	
WD1314−153	LHS 2712	···	···	14.81	3	14.90	3	14.98	3	V	0.007	16	82	15.17± 0.05	15.26± 0.09	15.32± 0.21	f
WD1327−083	LHS 354	12.42	6	12.33	6	12.44	5	12.49	6	···	···	···	···	12.62± 0.04	12.68± 0.04	12.74± 0.05	
WD1338+052	LSPM J1341+0500	···	···	16.71	3	16.02	3	15.41	3	R	0.006	20	58	14.74± 0.03	14.65± 0.03	14.61± 0.03	c
WD1339−340	PM J13420−3415	17.27	1	16.45	4	16.00	4	15.56	4	R	0.006	12	55	15.00± 0.04	14.75± 0.06	14.65± 0.10	f
WD1444−174	LHS 378	17.37	1	16.43	4	15.90	3	15.44	4	R	0.008	16	79	14.95± 0.03	14.64± 0.05	14.72± 0.11	
WD1447−190	LEHPM 2−1835	···	···	15.80	3	15.59	3	15.34	3	R	0.006	20	91	15.06± 0.04	14.87± 0.07	14.78± 0.11	f
WD1532+129	G137−24	16.48	2	15.70	2	15.34	2	15.09	2	···	···	···	···	14.94± 0.04	14.73± 0.05	14.71± 0.08	
WD1620−391	GJ 620.1B	···	···	11.04	3	11.15	3	11.29	3	R	0.008	15	73	11.58± 0.02	11.71± 0.02	11.77± 0.02	
WD1630+089	LSPM J1632+0851	15.71	3	15.08	3	14.70	3	14.31	3	R	0.007	12	56	13.85± 0.03	13.61± 0.03	13.49± 0.03	
WD1708−147	LP 747−11	14.39	1	14.32	1	14.21	1	14.14	1	···	···	···	···	··· ± ···	··· ± ···	··· ± ···	
WD1743−545	PM I17476-5436	···	···	16.28	3	15.66	3	15.10	3	R	0.010	13	57	14.46± 0.03	14.22± 0.05	14.29± 0.07	
WD1756+143	LSR J1758+1417	17.00	4	16.27	4	15.85	4	15.43	4	R	0.007	10	50	14.93± 0.04	14.66± 0.06	14.66± 0.08	f
WD1814+134	LSR J1817+1328	16.82	2	15.86	4	15.35	4	14.87	4	V	0.006	15	66	14.38± 0.04	14.10± 0.06	14.07± 0.06	f
WD1817−598	SCR 1821−5951	···	···	16.85	3	16.30	3	15.80	3	R	0.006	15	63	15.20± 0.05	15.01± 0.10	14.91± 0.14	b
WD1821−131	LHS 3384	16.11	4	15.56	4	15.21	1	14.79	4	···	···	···	···	··· ± ···	··· ± ···	··· ± ···	
WD1829+547	GJ 1228	16.06	2	15.53	2	···	···	15.04	2	···	···	···	···	14.80± 0.05	14.48± 0.05	14.51± 0.08	
WD1919−362	SCR 1920−3611	···	···	13.60	3	13.69	3	13.78	3	R	0.007	10	45	14.10± 0.03	14.22± 0.04	14.21± 0.07	
WD1917−077	GJ 754.1A	12.34	1	12.31	3	12.25	3	12.22	3	R	0.009	13	62	12.35± 0.03	12.36± 0.03	10.42± 0.03	
WD2028−171	LP 815−31	16.92	2	16.28	3	15.89	3	15.48	3	···	···	···	···	14.98± 0.04	14.79± 0.08	14.80± 0.10	
WD2035−369	L495−42	···	···	14.93	3	14.85	3	14.73	3	R	0.005	11	49	14.75± 0.04	14.72± 0.06	14.84± 0.09	f
WD2047+372	G210−36	13.07	3	13.00	3	13.08	3	13.11	3	···	···	···	···	13.30± 0.02	13.37± 0.02	13.43± 0.04	
···	WT 766	14.96	1	13.35	3	12.12	3	10.57	3	R	0.007	19	77	9.12± 0.03	8.48± 0.03	8.19± 0.02	
WD2057−493	PM I21010-4906	16.31	1	15.48	3	15.02	3	14.56	3	R	0.008	19	81	14.13± 0.03	13.86± 0.04	13.84± 0.05	
WD2105−820	GJ 820.1	···	···	13.62	3	13.58	3	13.50	3	R	0.008	13	52	13.48± 0.03	13.45± 0.03	13.53± 0.04	
WD2117+539	GJ 1261	12.41	3	12.35	3	12.43	3	12.48	3	···	···	···	···	12.68± 0.02	12.79± 0.02	12.85± 0.04	
WD2118−388	SCR 2122−3838	···	···	16.57	3	16.09	3	15.64	3	R	0.008	15	70	15.16± 0.04	14.92± 0.07	15.05± 0.12	h
WD2119+040	LSPM J2122+0413	17.75	2	16.78	3	16.28	3	15.81	3	···	···	···	···	15.24± 0.05	15.01± 0.07	14.88± 0.11	
WD2133−135	Ross 203	···	···	13.68	3	13.63	3	13.55	3	R	0.006	10	52	13.60± 0.03	13.58± 0.04	13.69± 0.06	b
WD2159−754	LHS 3752	···	···	15.04	3	14.93	3	14.80	3	R	0.005	13	57	14.72± 0.04	14.67± 0.07	14.55± 0.10	g
WD2211−392	LEHPM 1−4466	···	···	15.91	3	15.61	3	15.25	3	R	0.006	11	54	14.89± 0.03	14.64± 0.05	14.56± 0.08	f
WD2215+368	LP 287−39	18.31	2	17.16	2	16.55	2	15.98	2	···	···	···	···	15.41± 0.05	15.20± 0.10	14.97± 0.14	
WD2216−657	LHS 3794	···	···	14.55	3	14.47	3	14.41	3	R	0.006	14	62	14.54± 0.04	14.50± 0.06	14.53± 0.09	
WD2226−754B	SSSPM J2231−7514B	18.14	1	16.87	4	16.16	4	15.51	4	V	0.009	17	60	14.86± 0.04	14.82± 0.06	14.72± 0.12	f
WD2226−754A	SSSPM J2231−7514A	17.73	1	16.56	4	15.92	4	15.32	4	V	0.006	17	60	14.66± 0.04	14.66± 0.06	14.44± 0.08	f
WD2251−070	GJ 1276	···	···	15.70	3	15.11	3	14.56	3	R	0.006	29	153	14.01± 0.03	13.69± 0.04	13.55± 0.05	a
WD2307−691	LTT 9387B	13.66	1	13.57	1	13.55	1	13.50	1	···	···	···	···	13.60± 0.06	13.64± 0.10	13.66± 0.10	
WD2326+049	G29−38	13.17	2	13.04	2	···	···	13.01	2	···	···	···	···	13.13± 0.03	13.05± 0.03	12.55± 0.03	c
WD2341+322	G130−5	···	···	···	···	···	···	···	···	···	···	···	···	13.17± 0.03	13.20± 0.04	13.18± 0.03	
WD2352+401	LHS 4043	15.13	1	14.94	1	···	···	14.66	1	···	···	···	···	14.58± 0.04	14.45± 0.06	14.51± 0.09	

[a]Optical photometry values are adopted from Subasavage et al. (2009).

[b]Optical photometry values are adopted from Subasavage et al. (2008).

[c]JHK_S photometry has been transformed from the UKIDSS system using the transformations of Hodgkin et al. (2009) to the 2MASS system.

[d]Optical photometry values are adopted from Subasavage et al. (2007).

[e]Optical photometry values include additional measures than those presented in Subasavage et al. (2009) and, thus, supersede the values presented in that publication.

[f]Optical photometry values include additional measures than those presented in Subasavage et al. (2007) and, thus, supersede the values presented in that publication.

[g]ikely variable at the ∼1%−2% level.

[h]Optical photometry values include additional measures than those presented in Subasavage et al. (2008) and, thus, supersede the values presented in that publication.

[i]Variability analysis is contaminated by a nearby source, hence the brackets in Column 12 indicating erroneous variability.

[j]Optical magnitudes for this close binary ($\rho = 6\farcs3$ at P.A. 226.5°, epoch = 2014.91832) are uncertain because of the marginal calibrators for PSF photometry in the $6\farcm8^2$ FOV.

[k]JHK_S magnitudes are from NEWFIRM and are on the MKO system and, thus, represented with an italic font.

Table 2
CTIOPI Astrometric Results

Name (1)	R.A. (J2000.0) (2)	Decl. (J2000.0) (3)	Filter (4)	N_{sea} (5)	N_{frm} (6)	Coverage (7)	Years (8)	N_{ref} (9)	π(rel) (mas) (10)	π(corr) (mas) (11)	π(abs) (mas) (12)	μ (mas yr^{-1}) (13)	P.A. (deg) (14)	V_{tan} (km s^{-1}) (15)	Notes (16)
WD2359−434	00 02 10.73	−43 09 55.6	R	13s	142	2003.77−2015.83	12.06	7	120.12±0.88	1.25±0.19	121.37±0.90	886.8± 0.2	138.8±0.03	34.6	a
WD0000−345	00 02 40.10	−34 13 39.5	R	6s	61	2010.50−2015.84	5.34	8	69.36±1.41	1.03±0.12	70.39±1.42	766.5± 0.8	168.8±0.09	51.6	b,c
WD0011−721	00 13 49.91	−71 49 54.3	R	5s	66	2007.55−2011.97	4.42	8	52.15±1.10	0.62±0.03	52.77±1.10	335.7± 0.7	137.2±0.23	30.1	b
WD0034−602	00 36 22.32	−59 55 27.5	R	6s	59	2004.56−2009.92	5.36	10	40.24±1.56	1.17±0.14	41.41±1.57	276.8± 0.7	63.2±0.28	31.7	b
WD0038−226	00 41 26.03	−22 21 02.3	R	17s	133	1999.64−2015.82	16.19	7	110.05±0.86	1.24±0.07	111.29±0.86	608.0± 0.2	232.6±0.03	25.9	a
WD0046+051	00 49 09.91	+05 23 19.1	R	9s	77	2005.80−2015.96	10.16	6	230.87±1.56	1.25±0.09	232.12±1.56	2970.6± 0.4	156.9±0.02	60.7	
WD0123−460	01 25 18.04	−45 45 31.2	R	8s	63	2005.70−2012.94	7.24	9	42.61±1.88	0.28±0.03	42.89±1.88	744.2± 0.7	139.2±0.10	82.2	b
WD0127−311	01 29 56.13	−30 55 09.9	V	6g	59	1999.71−2011.73	12.02	5	18.04±1.19	1.11±0.08	19.15±1.19	120.6± 0.4	187.6±0.27	29.8	c
WD0141−675	01 43 00.98	−67 18 30.4	V	12g	163	2000.57−2015.82	15.25	6	100.92±0.79	0.88±0.07	101.80±0.79	1079.6± 0.2	199.2±0.01	50.3	a
WD0150+256	01 52 51.94	+25 53 40.7	R	6s	54	2003.95−2009.94	5.99	11	28.58±1.87	0.84±0.07	29.42±1.87	216.9± 0.8	76.7±0.38	35.0	
WD0222−291	02 24 32.30	−28 54 59.3	R	7c	44	2003.85−2010.01	6.15	8	28.36±2.67	0.54±0.07	28.90±2.67	485.3± 1.3	93.2±0.23	79.6	c
WD0226−329	02 28 27.20	−32 42 33.9	R	7s	53	2003.94−2010.73	6.80	9	20.80±1.29	1.00±0.13	21.80±1.30	227.4± 0.6	200.9±0.28	49.5	
WD0233−242	02 35 21.80	−24 00 47.3	R	6s	62	2007.74−2012.89	5.15	11	51.76±1.26	1.15±0.07	52.91±1.26	610.4± 0.7	191.1±0.11	54.7	b
WD0243−026	02 46 30.80	−02 27 23.3	R	7s	57	2010.01−2015.68	5.67	6	47.74±1.21	2.37±0.39	50.11±1.27	518.6± 0.7	155.8±0.14	49.1	b
WD0255−705	02 56 17.22	−70 22 10.9	R	6s	62	2004.98−2009.93	4.96	11	40.74±2.30	0.81±0.05	41.55±2.30	655.9± 1.1	100.8±0.16	74.8	b
WD0310−688	03 10 31.01	−68 36 03.4	R	7c	74	2008.86−2016.05	7.18	7	94.56±1.84	1.12±0.08	95.68±1.84	108.9± 1.0	166.6±0.89	5.4	
WD0311−649	03 12 25.69	−64 44 10.8	R	8s	69	2005.71−2012.89	7.19	9	30.01±1.20	0.75±0.06	30.76±1.20	168.1± 0.4	104.5±0.21	25.9	c
WD0326−273	03 28 48.79	−27 19 00.2	R	5s	57	2008.86−2012.94	4.08	7	40.29±1.82	0.78±0.38	41.07±1.86	826.8± 1.2	60.8±0.16	95.4	b,c
LHS1550	03 28 48.44	−27 19 04.7	R	5s	57	2008.86−2012.94	4.08	7	40.45±1.82	0.78±0.38	41.23±1.86	811.6± 1.2	61.1±0.16	93.3	
WD0344+014	03 47 06.83	+01 38 47.6	R	6s	61	2007.74−2012.94	5.20	9	49.91±1.07	0.55±0.06	50.46±1.07	461.3± 0.5	151.6±0.13	43.3	b
WD0435−088	04 37 47.41	−08 49 10.7	R	13s	137	2003.85−2015.93	12.07	10	105.26±1.36	1.01±0.06	106.27±1.36	1566.9± 0.3	171.5±0.02	69.9	
WD0548−001	05 51 19.49	−00 10 21.0	R	9s	93	2008.12−2015.83	7.71	12	88.17±0.92	1.51±0.18	89.68±0.94	255.3± 0.4	26.3±0.18	13.5	
WD0552−041	05 55 09.53	−04 10 07.1	R	13c	235	2003.94−2015.83	11.89	17	154.88±0.63	1.34±0.21	156.22±0.66	2374.5± 0.2	167.3±0.01	72.0	a,c
WD0651−398B	06 53 30.21	−39 54 29.1	R	6s	52	2006.22−2010.99	4.77	20	40.60±1.05	0.55±0.04	41.15±1.05	232.0± 0.7	343.8±0.28	26.7	b
WD0651−398A	06 53 35.34	−39 55 33.3	R	6s	52	2006.22−2010.99	4.77	22	39.81±1.02	0.54±0.04	40.35±1.02	230.8± 0.6	345.0±0.27	27.1	b
WD0655−390	06 57 05.90	−39 09 35.7	R	5s	48	2006.87−2010.99	4.12	12	58.05±0.88	0.74±0.07	58.79±0.88	335.1± 0.8	243.3±0.24	27.0	b
WD0659−063	07 01 54.84	−06 27 46.3	R	6s	57	2008.14−2012.83	4.69	10	44.21±1.13	1.10±0.13	45.31±1.14	889.1± 0.7	184.8±0.07	93.0	b
WD0708−670	07 08 52.28	−67 06 31.4	R	6c	59	2007.18−2011.96	4.78	11	58.31±1.01	1.04±0.08	59.35±1.01	246.5± 0.7	244.2±0.29	19.7	b
GJ283B	07 40 19.37	−17 24 45.9	I	12s	165	2003.96−2015.07	11.11	11	109.62±0.60	1.06±0.09	110.68±0.61	1272.6± 0.1	115.4±0.01	54.5	a
WD0738−172	07 40 20.78	−17 24 49.2	I	12s	165	2003.96−2015.07	11.11	11	109.34±0.60	1.06±0.09	110.40±0.61	1263.5± 0.1	115.9±0.01	54.2	a
WD0752−676	07 53 08.16	−67 47 31.5	R	13s	144	2003.95−2016.04	12.09	19	122.18±0.88	0.92±0.11	123.10±0.89	2096.4± 0.2	135.2±0.01	80.7	a
WD0816−310	08 18 40.26	−31 10 20.3	R	7s	49	2004.97−2010.96	5.99	7	51.57±0.71	0.73±0.05	52.30±0.71	827.1± 0.5	163.5±0.06	75.0	b
WD0821−669	08 21 26.71	−67 03 20.1	R	14s	184	2003.25−2016.05	12.80	11	94.07±0.54	0.64±0.05	94.71±0.54	760.9± 0.1	329.4±0.02	38.1	a
WD0839−327	08 41 32.43	−32 56 32.9	V	9g	91	2003.95−2016.05	12.10	16	116.36±1.04	1.66±0.17	118.02±1.05	1705.8± 0.2	322.3±0.01	68.5	a
WD0840−136	08 42 48.45	−13 47 13.1	R	8s	78	2006.21−2012.89	6.68	15	66.04±0.92	0.44±0.02	66.48±0.92	262.4± 0.5	264.3±0.17	18.7	b
LHS2067	08 53 56.35	−24 46 56.5	I	7s	71	2000.14−2012.10	11.96	16	39.21±0.60	0.63±0.08	39.84±0.61	635.2± 0.2	76.1±0.03	75.6	
WD0851−246	08 53 57.68	−24 46 56.2	I	7s	71	2000.14−2012.10	11.96	16	37.33±0.65	0.63±0.08	37.96±0.65	637.2± 0.2	76.4±0.03	79.6	c
WD0856−007	08 59 12.91	−00 58 42.9	R	7s	68	2007.19−2012.95	5.76	8	53.49±0.93	0.83±0.06	54.32±0.93	198.9± 0.5	126.6±0.30	17.4	b
WD1016−308	10 18 39.84	−31 08 02.1	R	6s	51	2004.17−2009.08	4.91	11	18.80±1.23	0.84±0.03	19.64±1.23	200.6± 0.6	295.1±0.34	48.4	
WD1036−204	10 38 55.57	−20 40 56.8	R	12s	117	2004.32−2016.05	11.73	8	69.26±0.56	0.68±0.04	69.94±0.56	609.5± 0.1	333.8±0.03	41.3	a,c
WD1105−340	11 07 47.89	−34 20 51.5	R	8s	93	2006.21−2013.38	7.18	7	37.92±0.92	1.62±0.10	39.54±0.93	265.2± 0.4	169.0±0.15	31.8	
SCR1107−3420B	11 07 50.25	−34 21 00.5	R	8s	93	2006.21−2013.38	7.18	7	36.91±0.94	1.62±0.10	38.53±0.95	262.9± 0.4	168.1±0.16	32.3	
WD1116−470	11 18 27.20	−47 21 57.0	R	5s	47	2007.19−2011.44	4.25	10	57.09±0.85	1.07±0.11	58.16±0.86	324.6± 0.6	276.5±0.16	26.5	b
WD1124−293	11 27 09.25	−29 40 11.2	R	7s	60	2010.16−2016.05	5.89	10	29.99±1.54	1.01±0.08	31.00±1.54	341.8± 0.7	141.3±0.25	52.3	
WD1142−645	11 45 42.93	−64 50 29.7	V	16s	214	2000.07−2015.39	15.33	10	215.37±1.17	1.64±0.19	217.01±1.19	2692.3± 0.3	97.5±0.01	58.8	a,d
WD1149−272	11 51 36.11	−27 32 21.1	R	10s	102	2004.18−2013.10	8.92	10	37.23±0.97	0.82±0.06	38.05±0.97	212.8± 0.4	283.2±0.18	26.5	
WD1202−232	12 05 26.68	−23 33 12.1	R	13s	132	2004.01−2016.06	12.05	8	90.26±0.72	1.62±0.12	91.88±0.73	245.6± 0.2	17.9±0.08	12.7	a
WD1236−495	12 38 49.78	−49 48 00.2	R	6c	63	2008.12−2013.51	5.39	11	64.77±0.75	0.83±0.06	65.60±0.75	551.9± 0.4	262.8±0.07	39.9	b
WD1237−230	12 40 24.18	−23 17 43.7	R	7s	47	2004.33−2010.21	5.88	8	24.90±2.10	0.47±0.03	25.37±2.10	1083.5± 0.7	223.8±0.07	202.4	c
WD1242−105	12 44 52.65	−10 51 08.8	V	7s	63	2004.17−2010.40	6.23	8	22.81±1.46	1.50±0.07	24.31±1.46	342.8± 0.7	259.3±0.18	66.9	c,d
WD1241−798	12 44 52.70	−80 09 27.9	V	5s	44	2005.21−2009.08	3.87	7	42.35±2.00	1.10±0.30	43.45±2.02	531.6± 1.7	312.5±0.38	58.0	b,c
WD1314−153	13 16 43.60	−15 35 58.3	V	7s	82	2003.10−2010.59	7.49	8	16.43±1.27	0.79±0.11	17.22±1.27	696.4± 0.5	197.3±0.07	191.7	c,d
WD1338+052	13 41 21.80	+05 00 45.8	R	7s	58	2009.10−2015.54	6.44	10	66.56±1.00	0.45±0.03	67.01±1.00	427.7± 0.6	273.3±0.12	30.3	b
WD1339−340	13 42 02.88	−34 15 19.4	R	3c	55	2006.21−2008.39	2.18	10	46.36±0.93	1.26±0.08	47.62±0.93	2562.1± 0.9	297.2±0.04	255.0	b,c
WD1444−174	14 47 25.34	−17 42 15.8	R	8s	79	2008.13−2015.39	7.26	9	72.63±0.91	0.52±0.05	73.15±0.91	1146.6± 0.4	253.7±0.04	74.3	
WD1447−190	14 50 11.93	−19 14 08.7	R	10s	91	2004.18−2013.38	9.20	9	19.31±0.84	1.77±0.16	21.08±0.86	266.4± 0.4	289.1±0.14	59.9	c
WD1620−391	16 23 33.83	−39 13 46.1	R	8s	73	2008.31−2015.29	6.98	13	76.27±1.50	1.60±0.20	77.87±1.51	80.1± 0.8	84.9±0.81	4.9	
WD1630+089	16 32 33.17	+08 51 22.7	R	6s	56	2010.52−2015.29	4.78	12	76.42±1.31	1.20±0.12	77.62±1.32	384.4± 0.7	130.9±0.22	23.5	b
WD1743−545	17 47 36.81	−54 36 31.2	R	6s	57	2010.40−2015.56	5.16	20	73.38±1.08	0.66±0.06	74.04±1.08	487.5± 0.7	231.4±0.17	31.2	b
WD1756+143	17 58 22.91	+14 17 37.9	R	4c	50	2009.31−2013.39	4.08	11	48.11±0.95	0.79±0.10	48.90±0.96	996.1± 0.9	236.6±0.10	96.6	b
WD1814+134	18 17 06.49	+13 28 25.0	V	8g	66	2003.52−2015.40	11.88	9	66.97±0.95	1.28±0.10	68.25±0.96	1195.1± 0.2	201.9±0.02	83.0	c
WD1817−598	18 21 59.54	−59 51 48.6	R	7s	63	2007.74−2013.38	5.64	10	33.49±0.59	0.58±0.07	34.07±0.59	359.9± 0.4	191.0±0.10	50.1	
WD1919−362	19 20 02.82	−36 11 02.7	R	5s	45	2006.53−2010.74	4.21	9	25.28±1.15	1.45±0.13	26.73±1.16	167.3± 0.9	139.5±0.58	29.7	

TABLE 2—*Continued*

Name (1)	R.A. (J2000.0) (2)	Decl. (J2000.0) (3)	Filter (4)	N_{sea} (5)	N_{frm} (6)	Coverage (7)	Years (8)	N_{ref} (9)	π(rel) (mas) (10)	π(corr) (mas) (11)	π(abs) (mas) (12)	μ (mas yr^{-1}) (13)	P.A. (deg) (14)	V_{tan} (km s^{-1}) (15)	Notes (16)
WD1917−077	19 20 34.92	−07 40 00.0	R	7s	62	2009.32−2015.40	6.08	10	96.38±0.81	1.60±0.20	97.98±0.83	167.9± 0.5	201.1±0.29	8.1	
WD2035−369	20 38 41.42	−36 49 13.5	R	5s	49	2004.44−2009.78	5.34	7	29.69±0.98	1.62±0.24	31.31±1.01	218.4± 0.6	103.7±0.28	33.1	
LEP2101−4906A	21 01 07.41	−49 07 24.9	R	6c	77	2010.40−2015.56	5.16	11	75.07±1.07	0.66±0.06	75.73±1.07	364.1± 0.6	234.7±0.20	22.7	
WD2057−493	21 01 05.21	−49 06 24.2	R	6c	81	2010.40−2015.56	5.16	11	74.47±1.03	0.66±0.06	75.13±1.03	368.6± 0.6	234.0±0.19	23.3	b,c
WD2105−820	21 13 16.81	−81 49 12.8	R	7s	52	2009.54−2015.37	5.82	10	64.30±1.41	0.67±0.08	64.97±1.41	452.0± 0.8	144.9±0.20	33.0	b
WD2118−388	21 22 05.59	−38 38 34.8	R	8s	70	2007.74−2014.45	6.71	10	43.01±1.32	0.55±0.05	43.56±1.32	176.8± 0.7	108.6±0.39	19.2	b
WD2133−135	21 36 16.39	−13 18 34.5	R	4s	52	2006.37−2010.82	4.45	9	39.75±1.28	0.81±0.09	40.56±1.28	293.6± 0.6	117.2±0.23	34.3	b
WD2159−754	22 04 20.84	−75 13 26.1	R	6s	57	2007.56−2012.51	4.95	10	49.28±1.22	0.95±0.10	50.23±1.22	539.8± 0.7	278.5±0.13	50.9	b,c
WD2211−392	22 14 34.75	−38 59 07.3	R	6s	54	2005.71−2010.65	4.94	8	52.55±1.15	0.78±0.08	53.33±1.15	1075.3± 0.6	110.1±0.06	95.6	
WD2216−657	22 19 48.32	−65 29 17.6	R	7s	62	2004.90−2011.71	6.81	10	38.15±1.52	0.84±0.07	38.99±1.52	672.2± 0.7	163.7±0.10	81.7	
WD2226−754B	22 30 33.55	−75 15 24.2	V	6s	60	2002.51−2007.60	5.09	10	64.53±1.40	0.67±0.07	65.20±1.40	1867.3± 1.0	167.3±0.05	135.8	b,c,d
WD2226−754A	22 30 40.00	−75 13 55.3	V	6s	60	2002.51−2007.60	5.09	10	64.68±1.41	0.67±0.07	65.35±1.41	1857.6± 1.0	167.8±0.05	134.7	b,c,d
WD2251−070	22 53 53.35	−06 46 54.4	R	12s	153	2003.52−2015.83	12.31	8	115.28±0.81	1.49±0.14	116.77±0.82	2572.9± 0.2	105.4±0.01	104.4	a

[a] Astrometric determinations presented here supersede those of Subasavage et al. (2009) because they include additional data over ∼6 years (see Section 3).

[b] New member of the 25 pc WD sample.

[c] Object is discussed in Section 4.2.

[d] Both oV and nV data were used to determine the astrometric solution as described in Section 2.3.1.

Table 3
NOFS Astrometric Results

Name (1)	R.A. (J2000.0) (2)	Decl. (J2000.0) (3)	Filter (4)	N_{ngt} (5)	N_{frm} (6)	Coverage (7)	Years (8)	N_{ref} (9)	π(rel) (mas) (10)	π(corr) (mas) (11)	π(abs) (mas) (12)	μ (mas yr^{-1}) (13)	P.A. (deg) (14)	V_{tan} (km s^{-1}) (15)	CCD (16)	Notes (17)
WD0008+424	00 11 22.46	+42 40 40.9	A2-1	67	113	2008.57−2011.97	3.40	8	42.59±0.30	0.58±0.05	43.17±0.30	229.3± 0.2	191.8±0.04	25.2	EEV24	a
WD0025+054	00 27 36.64	+05 42 03.2	A2-1	53	67	2012.62−2016.00	3.38	19	44.07±0.44	1.03±0.07	45.10±0.45	365.2± 0.2	134.3±0.04	38.4	EEV24	a
WD0038−226	00 41 26.03	−22 21 02.3	A2-1	49	55	1992.79−1996.95	4.16	5	108.76±0.70	1.51±0.13	110.27±0.71	604.8± 0.5	232.9±0.05	26.0	Tek2K	
WD0053−117	00 55 50.33	−11 27 31.6	A2-1	56	67	1992.79−1996.98	4.19	4	42.89±0.38	0.89±0.09	43.78±0.39	456.9± 0.2	348.4±0.02	49.5	Tek2K	a
WD0136+152	01 38 56.87	+15 27 42.2	A2-1	78	101	1992.67−1996.98	4.30	14	43.24±0.58	1.72±0.10	44.96±0.59	99.6± 0.3	207.3±0.14	10.5	Tek2K	a
WD0148+641	01 51 51.26	+64 25 52.7	A2-1	50	69	2012.61−2016.00	3.39	28	57.61±0.40	0.88±0.19	58.49±0.44	302.0± 0.3	132.0±0.05	24.5	EEV24	
WD0213+396	02 16 16.36	+39 51 25.4	ST-R	35	70	1990.78−1995.82	5.03	5	49.92±0.82	0.83±0.07	50.75±0.82	186.0± 0.4	240.4±0.14	17.4	TI800	a
WD0236+259	02 39 19.67	+26 09 57.6	A2-1	93	113	2008.72−2015.06	6.34	16	46.41±0.28	0.68±0.05	47.09±0.28	355.0± 0.1	117.8±0.02	35.7	EEV24	a
WD0243−026	02 46 30.80	−02 27 23.3	A2-1	60	72	1992.67−1997.03	4.35	6	45.70±0.52	1.77±0.13	47.47±0.54	511.0± 0.3	155.6±0.03	51.0	Tek2K	a
WD0322−019	03 25 11.05	−01 49 15.1	A2-1	82	104	1992.75−1997.09	4.34	7	56.76±0.32	0.95±0.07	57.71±0.33	890.4± 0.2	165.3±0.01	73.1	Tek2K	b
WD0423+044	04 26 20.70	+04 32 30.6	A2-1	173	233	1992.80−2003.01	10.21	11	47.55±0.26	1.08±0.11	48.63±0.28	845.1± 0.1	132.8±0.01	82.4	Tek2K	
WD0457−004	04 59 43.23	−00 22 39.0	A2-1	79	133	2008.72−2012.95	4.23	19	39.43±0.22	0.72±0.05	40.15±0.23	286.0± 0.1	142.2±0.03	33.8	EEV24	a
WD0511+079	05 14 03.49	+08 00 15.2	A2-1	66	68	1992.14−1997.12	4.98	5	45.36±0.42	0.45±0.04	45.81±0.42	378.9± 0.3	216.4±0.03	39.2	Tek2K	
WD0644+025	06 47 22.15	+02 31 08.9	A2-1	53	117	2012.93−2016.09	3.16	47	54.00±0.31	0.95±0.05	54.95±0.31	411.8± 0.2	274.1±0.05	35.5	EEV24	a
WD0659−063	07 01 54.84	−06 27 46.3	A2-1	89	285	2008.79−2013.10	4.31	29	47.45±0.22	1.01±0.06	48.46±0.23	889.2± 0.2	184.5±0.01	87.0	EEV24	a
WD0728+642	07 33 30.88	+64 09 27.4	A2-1	129	192	1996.83−2003.01	6.18	13	49.96±0.29	0.85±0.06	50.81±0.30	258.4± 0.2	171.6±0.02	24.1	Tek2K	a
WD0802+387	08 05 57.66	+38 33 44.7	A2-1	39	43	1992.14−1996.23	4.09	10	48.17±0.56	0.89±0.06	49.06±0.56	832.5± 0.4	228.9±0.03	80.4	Tek2K	b
WD0810+489	08 14 11.17	+48 45 29.8	A2-1	69	74	2008.23−2013.05	4.81	16	58.14±0.32	0.86±0.05	59.00±0.32	257.8± 0.2	165.7±0.04	20.7	Tek2K	a
WD1008+290	10 11 41.58	+28 45 59.1	A2-1	87	94	1998.30−2003.02	4.72	12	66.76±0.45	0.78±0.06	67.54±0.45	720.4± 0.3	190.4±0.02	50.6	Tek2K	a,b
WD1033+714	10 37 02.71	+71 10 58.9	A2-1	29	32	1992.27−1996.32	4.05	9	56.03±0.61	0.98±0.07	57.01±0.61	1915.2± 0.3	256.4±0.02	159.2	Tek2K	a
WD1036−204	10 38 55.57	−20 40 56.8	A2-1	42	42	2003.26−2008.17	4.90	16	69.13±0.66	1.00±0.06	70.13±0.66	620.0± 0.5	333.9±0.03	41.9	Tek2K	
WD1313−198	13 16 19.57	−20 07 32.1	ST-R	25	32	1991.03−1995.41	4.38	6	42.46±0.74	0.69±0.07	43.15±0.74	629.3± 0.3	274.4±0.04	69.1	TI800	a
WD1327−083	13 30 13.64	−08 34 29.4	I-2	22	24	2013.20−2016.43	3.23	8	60.91±1.34	1.18±0.09	62.09±1.34	1196.6± 0.7	247.6±0.04	91.3	EEV24	
WD1444−174	14 47 25.35	−17 42 15.8	A2-1	43	44	1992.27−1997.28	5.02	13	73.59±0.72	0.61±0.05	74.20±0.72	1145.0± 0.3	253.0±0.02	73.1	Tek2K	
WD1532+129	15 35 05.81	+12 47 45.2	A2-1	31	35	2012.38−2015.48	3.10	13	51.67±0.72	0.68±0.05	52.35±0.72	238.7± 0.5	223.3±0.11	21.6	EEV24	a
WD1708−147	17 11 26.77	−14 47 53.6	A2-1	70	97	2008.26−2012.48	4.22	23	41.95±0.53	1.65±0.09	43.60±0.54	388.3± 0.3	134.8±0.04	42.2	Tek2K	a
WD1756+143	17 58 22.91	+14 17 37.9	A2-1	108	167	2008.25−2012.63	4.38	29	46.63±0.27	0.91±0.06	47.54±0.28	996.8± 0.1	236.4±0.01	99.4	Tek2K	a
WD1814+134	18 17 06.49	+13 28 25.0	A2-1	72	102	2008.29−2012.47	4.18	12	65.33±0.28	0.72±0.05	66.05±0.28	1194.9± 0.2	201.4±0.01	85.7	EEV24	
WD1821−131	18 24 04.54	−13 08 42.2	A2-1	54	63	1992.31−1996.56	4.24	4	52.58±0.56	1.00±0.30	53.58±0.64	669.9± 0.3	198.3±0.02	59.3	Tek2K	a
WD1829+547	18 30 20.28	+54 47 27.2	A2-1	94	164	1998.54−2001.55	3.01	16	57.44±0.36	0.91±0.05	58.35±0.36	393.2± 0.3	318.3±0.04	31.9	Tek2K	
WD2028−171	20 31 09.58	−16 58 41.9	A2-1	55	82	2012.39−2015.79	3.40	28	43.59±0.54	0.63±0.04	44.22±0.54	199.1± 0.5	290.7±0.09	21.3	EEV24	a,b
WD2047+372	20 49 06.71	+37 28 14.1	Z-2	79	171	2008.43−2012.47	4.04	30	57.12±0.29	1.50±0.11	58.62±0.31	223.7± 0.2	47.4±0.04	18.1	EEV24	
WD2117+539	21 18 56.27	+54 12 41.5	I-2	46	61	2012.61−2015.79	3.17	16	56.42±0.61	0.94±0.58	57.36±0.84	212.1± 0.4	337.1±0.09	17.5	EEV24	
WD2119+040	21 22 12.35	+04 13 56.8	A2-1	51	59	2012.61−2015.79	3.17	24	40.49±0.52	0.70±0.04	41.19±0.52	414.2± 0.3	190.5±0.04	47.7	EEV24	a
WD2215+368	22 17 47.60	+37 07 51.0	A2-1	76	127	2008.49−2012.87	4.37	39	48.71±0.28	0.48±0.03	49.19±0.28	469.7± 0.1	78.5±0.02	45.3	EEV24	a
WD2326+049	23 28 47.62	+05 14 54.2	I-2	136	192	1999.61−2005.76	6.15	16	55.77±0.39	1.06±0.06	56.83±0.39	480.5± 0.1	237.8±0.02	40.1	Tek2K	b
WD2341+322	23 43 50.72	+32 32 46.8	I-2	67	117	2012.70−2015.79	3.09	19	52.28±0.41	0.77±0.05	53.05±0.41	219.6± 0.2	255.6±0.07	19.6	EEV24	
WD2352+401	23 54 56.26	+40 27 29.5	A2-1	99	122	2003.59−2007.97	4.38	21	44.21±0.35	0.93±0.06	45.14±0.36	566.2± 0.2	159.1±0.02	59.5	Tek2K	a

[a] New member of the 25 pc WD sample.

[b] Object is discussed in Section 4.2.

Table 4
Physical Parameters

WD Name (1)	Adopted π[a] (mas) (2)	No. of π (3)	Ref. (4)	$T_{\rm eff}$ (K) (5)	log g (6)	Spectral Type (7)	Ref. (8)	Comp (9)	$M/M_{\odot}$ (10)	M_V (11)	log $L/L_{\odot}$ (12)	Age[b] (Gyr) (13)	Notes (14)
WD2359−434	121.47±0.89	2	1,2	8390± 170	8.37± 0.02	DAP	16	H	0.83± 0.02	13.39±0.03	−3.36± 0.04	1.83± 0.18	
WD0000−345	70.52±1.40	2	1,2	6280± 100	8.18± 0.03	DC	17	He	0.68± 0.03	14.27±0.05	−3.76± 0.04	3.23± 0.35	
WD0008+424	43.17±0.30	1	3	7020± 150	7.99± 0.04	DA	18	H	0.58± 0.03	13.50±0.03	−3.44± 0.01	1.48± 0.02	c,d
WD0011−721	52.77±1.10	1	1	6340± 150	7.89± 0.04	DA	19	H	0.53± 0.04	13.78±0.05	−3.57± 0.05	1.66± 0.14	
WD0025+054	45.10±0.45	1	3	5650± 60	7.97± 0.02	DA	20	H	0.57± 0.02	14.42±0.04	−3.81± 0.02	2.61± 0.17	
WD0034−602	41.41±1.57	1	1	14540± 810	8.54± 0.05	DA	21	H	0.95± 0.04	12.17±0.09	−2.52± 0.10	0.52± 0.10	
WD0038−226	110.66±0.55	3	1,2,3	5230± 60	7.92± 0.03	DQpec	22	He(+H)	0.52± 0.03	14.71±0.03	−3.94± 0.03	4.23± 0.34	e
WD0046+051	232.37±1.18	3	1,2,4	6130± 110	8.16± 0.03	DZ	23	He(+H,Ca)	0.67± 0.02	14.21±0.03	−3.79± 0.04	3.45± 0.36	f
WD0053−117	43.77±0.39	1	3	7080± 140	7.99± 0.03	DA	24	H	0.58± 0.03	13.45±0.04	−3.43± 0.04	1.45± 0.10	
WD0123−460	42.89±1.88	1	1	5810± 160	8.10± 0.07	DA	19	H	0.65± 0.06	14.46±0.10	−3.84± 0.07	3.19± 0.73	
WD0127−311	19.15±1.19	1	1	10910± 830	8.06± 0.11	DB	25	He	0.62± 0.10	12.15±0.14	−2.73± 0.15	0.54± 0.16	
WD0136+152	44.96±0.59	1	3	7940± 120	8.11± 0.02	DA	24	H	0.66± 0.02	13.20±0.04	−3.30± 0.03	1.29± 0.07	
WD0141−675	101.80±0.79	1	1	6380± 120	7.97± 0.03	DAZ	26	H	0.57± 0.03	13.86±0.02	−3.60± 0.04	1.82± 0.13	
WD0148+641	58.02±0.30	2	3,5	8660± 390	8.05± 0.08	DA	24	H	0.63± 0.07	12.79±0.03	−3.11± 0.09	0.94± 0.18	
WD0150+256	29.42±1.87	1	1	7720± 280	7.93± 0.09	DA	27	H	0.55± 0.08	13.05±0.13	−3.25± 0.09	1.07± 0.18	
WD0213+396	50.75±0.82	1	3	9000± 210	8.35± 0.04	DA	24	H	0.82± 0.03	13.10±0.05	−3.22± 0.05	1.38± 0.16	
WD0222−291	28.90±2.67	1	1	··· ± ···	··· ± ···	DC	28	···	··· ± ···	15.35±0.21	··· ± ···	··· ± ···	
WD0226−329	21.80±1.30	1	1	22140±1610	7.97± 0.09	DA	24	H	0.61± 0.07	10.55±0.13	−1.41± 0.14	0.04± 0.02	
WD0233−242	52.91±1.26	1	1	5270± 110	7.77± 0.06	DC	18	H	0.45± 0.04	14.56±0.06	−3.83± 0.05	2.38± 0.41	
WD0236+259	47.09±0.28	1	3	5580± 20	7.98± 0.01	DA	27	H	0.57± 0.01	14.50±0.04	−3.84± 0.01	2.80± 0.10	c,g
WD0243−026	47.87±0.49	3	1,2,3	6890± 140	8.23± 0.03	DAZ	29	H	0.73± 0.03	13.93±0.04	−3.62± 0.04	2.46± 0.29	
WD0255−705	41.55±2.30	1	1	10480± 320	8.10± 0.07	DA	24	H	0.66± 0.06	12.16±0.12	−2.81± 0.08	0.61± 0.08	
WD0310−688	96.58±1.30	3	1,2,4	15460±1030	8.06± 0.04	DA	24	H	0.65± 0.04	11.30±0.04	−2.10± 0.11	0.20± 0.05	
WD0311−649	30.76±1.20	1	1	11760± 700	7.28± 0.05	DA	19	H	0.29± 0.02	10.72±0.09	−2.14± 0.11	0.19± 0.04	h
WD0322−019	57.73±0.33	2	3,6	5300± 70	8.12± 0.04	DAZH	29,30	H	0.66± 0.03	14.94±0.03	−4.01± 0.04	5.52± 0.53	h
WD0326−273	41.30±1.31	3	1,2,7	8740± 370	7.29± 0.08	DA	29	H	0.28± 0.04	11.69±0.08	−2.69± 0.09	0.43± 0.06	h
WD0344+014	50.46±1.07	1	1	4990± 100	7.93± 0.06	DC	21	He	0.53± 0.05	15.02±0.05	−4.02± 0.05	5.09± 0.50	
WD0423+044	48.63±0.28	2	3,8	4860± 70	8.22± 0.04	DA	17	H	0.72± 0.04	15.57±0.03	−4.22± 0.04	8.23± 0.33	
WD0435−088	106.04±1.21	2	1,2	6290± 120	7.92± 0.03	DQ	31	He(+C)	0.53± 0.03	13.88±0.04	−3.61± 0.04	1.86± 0.14	i
WD0457−004	40.15±0.23	1	3	11260± 180	8.81± 0.02	DA	24	H	1.10± 0.01	13.18±0.04	−3.17± 0.03	1.80± 0.07	c,g
WD0511+079	46.08±0.40	2	3,8	6830± 140	8.39± 0.04	DA	24	H	0.84± 0.03	14.19±0.04	−3.74± 0.05	3.59± 0.24	
WD0548−001	89.74±0.89	2	1,2	6170± 70	8.20± 0.02	DQP	22	He(+C)	0.70± 0.02	14.36±0.04	−3.80± 0.03	3.67± 0.24	j
WD0552−041	156.11±0.63	2	1,2	5430± 90	8.49± 0.03	DZ	23	H	0.90± 0.02	15.44±0.03	−4.20± 0.04	7.34± 0.36	k
WD0644+025	54.95±0.31	2	2,3	7200± 100	8.61± 0.02	DA	24	H	0.99± 0.01	14.37±0.03	−3.79± 0.03	3.90± 0.11	
WD0651−398B	40.74±0.73	2	1,7	6360± 220	8.14± 0.06	DA	19	H	0.68± 0.05	14.12±0.05	−3.70± 0.07	2.66± 0.52	
WD0651−398A	40.74±0.73	2	1,7	7100± 220	8.03± 0.05	DA	19	H	0.61± 0.05	13.51±0.05	−3.45± 0.06	1.53± 0.17	
WD0655−390	58.79±0.88	1	1	6310± 160	8.01± 0.04	DA	19	H	0.60± 0.04	13.96±0.04	−3.64± 0.05	2.01± 0.24	
WD0659−063	48.34±0.23	3	1,2,3	6590± 140	8.07± 0.03	DA	24	H	0.63± 0.03	13.86±0.03	−3.60± 0.04	2.01± 0.18	
WD0708−670	59.35±1.01	1	1	5020± 80	7.99± 0.04	DC	19	He	0.56± 0.03	15.09±0.05	−4.04± 0.04	5.47± 0.34	
WD0728+642	50.81±0.30	1	3	5210± 60	7.92± 0.03	DAP	22	H	0.53± 0.03	14.75±0.03	−3.93± 0.03	3.62± 0.46	
WD0738−172	110.59±0.43	3	1,2,7	7700± 210	8.05± 0.03	DZA	22	He(+H,Ca)	0.61± 0.03	13.28±0.03	−3.33± 0.05	1.31± 0.11	l
WD0752−676	123.30±0.89	2	1,2	5620± 90	7.96± 0.03	DA	24	H	0.56± 0.02	14.41±0.03	−3.82± 0.04	2.61± 0.26	
WD0802+387	48.71±0.49	2	3,9	4990± 70	8.19± 0.04	DA	20	H	0.70± 0.04	15.33±0.04	−4.16± 0.04	7.54± 0.37	
WD0810+489	59.00±0.32	1	3	6440± 170	8.05± 0.04	DC	18	He	0.60± 0.04	13.92±0.03	−3.64± 0.05	2.09± 0.31	
WD0816−310	52.30±0.71	1	1	6480± 290	8.22± 0.07	DZ	19	He(+H,Ca)	0.71± 0.06	14.02±0.04	−3.73± 0.09	3.19± 0.71	m
WD0821−669	94.71±0.54	1	1	5060± 100	8.12± 0.04	DA	21	H	0.65± 0.04	15.22±0.03	−4.09± 0.04	6.68± 0.53	
WD0839−327	117.96±1.04	2	1,2	9040± 190	7.77± 0.03	DA	24	H	0.47± 0.02	12.22±0.04	−2.88± 0.04	0.59± 0.04	
WD0840−136	66.48±0.92	1	1	4980± 230	7.95± 0.10	DZ	21	He(+H,Ca)	0.54± 0.08	14.83±0.04	−4.04± 0.10	5.28± 0.84	n
WD0851−246	38.96±0.44	2	1,7	3490± 80	7.89± 0.05	DC	32	He(+H)	0.50± 0.05	16.05±0.02	−4.63± 0.06	8.06± 0.28	
WD0856−007	54.32±0.93	1	1	5240± 90	8.10± 0.04	DC	19	H	0.64± 0.03	15.00±0.05	−4.02± 0.04	5.62± 0.62	
WD1008+290	67.54±0.45	1	3	4140± 40	8.00± 0.04	DQpecP	22	He	0.57± 0.03	16.66±0.03	−4.38± 0.03	7.29± 0.22	o
WD1016−308	19.64±1.23	1	1	14990± 960	7.92± 0.09	DA	21	H	0.57± 0.07	11.15±0.14	−2.07± 0.12	0.17± 0.05	
WD1033+714	57.01±0.61	1	3	4740± 70	8.22± 0.04	DC	22	H	0.72± 0.04	15.72±0.04	−4.27± 0.04	8.60± 0.29	
WD1036−204	70.02±0.43	2	1,3	5300± 80	8.32± 0.03	DQpecP	22	He	0.78± 0.03	15.48±0.03	−4.14± 0.04	6.52± 0.19	o
WD1105−340	39.04±0.66	2	1,7	13810± 990	8.14± 0.05	DA	21	H	0.69± 0.04	11.62±0.05	−2.34± 0.12	0.31± 0.07	
WD1116−470	58.16±0.86	1	1	5810± 140	8.02± 0.05	DC	19	He	0.58± 0.04	14.34±0.04	−3.81± 0.05	3.19± 0.57	
WD1124−293	31.00±1.54	1	1	9150± 220	7.99± 0.06	DAZ	29	H	0.59± 0.05	12.50±0.11	−2.98± 0.07	0.75± 0.09	
WD1142−645	215.86±0.26	4	1,2,4,5	7880± 180	8.04± 0.03	DQ	31	He(+C)	0.60± 0.02	13.17±0.03	−3.28± 0.05	1.21± 0.09	p
WD1149−272	38.05±0.97	1	1	6280± 200	7.86± 0.07	DQ	21	He(+C)	0.49± 0.05	13.77±0.06	−3.58± 0.07	1.74± 0.22	q
WD1202−232	91.88±0.73	1	1	8520± 170	7.89± 0.03	DAZ	29	H	0.53± 0.02	12.62±0.03	−3.05± 0.04	0.79± 0.05	
WD1236−495	65.57±0.75	2	1,2	10780± 270	8.59± 0.03	DAV	22	H	0.98± 0.02	12.89±0.04	−3.08± 0.05	1.43± 0.15	
WD1237−230	25.37±2.10	1	1	5670± 90	7.29± 0.11	DA	24	H	0.26± 0.05	13.56±0.18	−3.46± 0.08	1.21± 0.10	h
WD1242−105	25.17±0.77	2	1,10	7910± 180	7.02± 0.05	DA	18	H	0.21± 0.02	11.73±0.07	−2.72± 0.05	0.45± 0.03	h

TABLE 4—*Continued*

WD Name (1)	Adopted π[a] (mas) (2)	No. of π (3)	Ref. (4)	$T_{\rm eff}$ (K) (5)	log g (6)	Spectral Type (7)	Ref. (8)	Comp (9)	$M/M_{\odot}$ (10)	M_V (11)	log $L/L_{\odot}$ (12)	Age[b] (Gyr) (13)	Notes (14)
WD1241−798	43.45±2.02	1	1	5550± 150	7.88±0.08	DC	33	He	0.50±0.06	14.37±0.11	−3.81±0.07	2.84±0.73	
WD1313−198	43.15±0.74	1	3	4640± 80	8.03±0.05	DZ	23	He(+H,Ca)	0.59±0.05	15.33±0.05	−4.20±0.05	6.58±0.36	r
WD1314−153	17.22±1.27	1	1	15700±2240	7.86±0.14	DA	24	H	0.54±0.11	10.99±0.16	−1.95±0.24	0.13±0.10	
WD1327−083	62.34±1.17	4	2,3,4,11	13990± 660	7.94±0.04	DA	24	H	0.58±0.03	11.30±0.04	−2.21±0.09	0.22±0.04	
WD1338+052	67.01±1.00	1	1	4280± 70	7.89±0.05	DC	34	H	0.51±0.04	15.84±0.04	−4.26±0.04	7.19±0.56	
WD1339−340	47.62±0.93	1	1	5230± 70	7.99±0.04	DA	35	H	0.58±0.04	14.84±0.05	−3.96±0.04	4.41±0.65	
WD1444−174	73.70±0.56	3	1,2,3	5040± 60	8.49±0.03	DC	22	H	0.90±0.02	15.77±0.03	−4.33±0.03	8.60±0.14	
WD1447−190	21.08±0.86	1	1	7070± 220	7.18±0.07	DA	27	H	0.24±0.03	12.42±0.09	−3.01±0.07	0.68±0.06	h
WD1532+129	52.35±0.72	1	3	5430± 70	7.90±0.03	DZ	36	He(+H,Ca)	0.51±0.03	14.29±0.03	−3.86±0.03	3.36±0.35	s
WD1620−391	78.15±0.36	5	1,2,4,11,12	23280±1760	8.00±0.05	DA	24	H	0.63±0.04	10.50±0.03	−1.34±0.13	0.03±0.02	
WD1630+089	77.62±1.32	1	1	5670± 60	8.07±0.03	DA	34	H	0.63±0.03	14.53±0.05	−3.86±0.03	3.20±0.32	
WD1708−147	43.56±0.54	2	2,3	9280± 370	7.93±0.06	DQ	31	He(+C)	0.54±0.05	12.52±0.03	−2.93±0.08	0.69±0.10	t
WD1743−545	74.04±1.08	1	1	4530± 120	7.97±0.06	DC	33	H	0.56±0.05	15.63±0.04	−4.21±0.06	7.21±0.68	
WD1756+143	47.65±0.27	2	1,3	5440± 70	8.01±0.04	DA	37	H	0.59±0.03	14.66±0.03	−3.90±0.03	3.50±0.51	
WD1814+134	66.42±0.26	3	1,3,13	5020± 60	7.94±0.03	DA	37	H	0.55±0.03	14.97±0.03	−4.01±0.03	4.83±0.53	
WD1817−598	34.07±0.59	1	1	4950± 130	7.44±0.08	DC	19	H	0.30±0.05	14.51±0.05	−3.79±0.06	2.11±0.32	
WD1821−131	53.58±0.59	1	3	5930± 130	7.97±0.05	DAZ	29	H	0.57±0.05	14.21±0.03	−3.73±0.05	2.21±0.30	
WD1829+547	58.38±0.36	2	2,3	6330± 120	8.31±0.04	DXP	22	He	0.78±0.03	14.36±0.03	−3.83±0.04	4.01±0.31	
WD1919−362	26.74±1.16	1	1	23360±7640	8.17±0.09	DB	19	He	0.70±0.08	10.74±0.10	−1.46±0.49	0.05±0.18	
WD1917−077	95.84±0.40	4	1,2,4,5	11220± 300	8.15±0.03	DBQA	22	He	0.67±0.02	12.22±0.03	−2.73±0.05	0.57±0.05	
WD2028−171	44.22±0.54	1	3	5640± 90	8.03±0.04	DAZ	33	H	0.60±0.03	14.51±0.03	−3.85±0.04	2.96±0.39	
WD2035−369	31.31±1.01	1	1	9610± 300	8.05±0.06	DA	21	H	0.63±0.05	12.41±0.08	−2.93±0.07	0.72±0.09	
WD2047+372	58.49±0.28	2	3,8	14600± 590	8.33±0.03	DA	24	H	0.82±0.02	11.84±0.03	−2.37±0.07	0.36±0.05	
WD2057−493	75.42±0.74	2	1,7	5320± 60	8.09±0.03	DA	33	H	0.64±0.03	14.88±0.04	−3.99±0.03	5.03±0.48	
WD2105−820	64.81±1.39	2	1,2	9820± 240	8.29±0.04	DAZH	22	H	0.78±0.03	12.68±0.06	−3.04±0.05	0.98±0.09	
WD2117+539	57.56±0.53	3	2,3,5	15250± 660	7.94±0.03	DA	24	H	0.58±0.03	11.16±0.03	−2.05±0.08	0.17±0.03	
WD2118−388	43.56±1.32	1	1	5150± 110	7.86±0.06	DC	19	He	0.49±0.05	14.77±0.07	−3.93±0.06	4.01±0.61	
WD2119+040	41.19±0.52	1	3	4970± 70	7.80±0.04	DA	34	H	0.47±0.03	14.85±0.04	−3.95±0.04	3.66±0.48	
WD2133−135	40.56±1.28	1	1	10060± 270	7.69±0.05	DA	19	H	0.44±0.03	11.72±0.07	−2.65±0.06	0.41±0.04	
WD2159−754	50.23±1.22	1	1	8900± 320	8.59±0.05	DA	24	H	0.97±0.04	13.54±0.06	−3.41±0.07	2.39±0.27	
WD2211−392	53.36±1.05	2	1,14	6120± 160	8.33±0.05	DA	21	H	0.80±0.04	14.55±0.05	−3.88±0.06	4.27±0.39	
WD2215+368	49.19±0.28	1	3	4530± 60	7.98±0.04	DC	27	H	0.56±0.04	15.62±0.03	−4.21±0.04	7.26±0.44	
WD2216−657	38.99±1.52	1	1	9770± 660	8.09±0.10	DZ	38	He(+H,Ca)	0.63±0.09	12.50±0.09	−2.93±0.13	0.75±0.19	u
WD2226−754B	65.27±0.99	2	1,7	4200± 70	7.89±0.05	DC	39	H	0.51±0.04	15.95±0.04	−4.30±0.04	7.41±0.52	
WD2226−754A	65.27±0.99	2	1,7	4410± 60	7.87±0.05	DC	39	H	0.50±0.04	15.63±0.04	−4.20±0.04	6.50±0.55	
WD2251−070	117.01±0.81	2	1,2	4000± 200	7.92±0.01	DZ	23	He(+Ca)	0.52±0.01	16.04±0.03	−4.40±0.01	7.13±0.08	v
WD2307−691	47.51±0.19	2	4,15	10910± 470	7.93±0.06	DB	33	He	0.54±0.05	11.96±0.03	−2.65±0.08	0.45±0.07	
WD2326+049	56.99±0.39	2	2,3	11240± 360	8.00±0.03	DAZV	40,41	H	0.60±0.03	11.82±0.03	−2.62±0.06	0.44±0.04	
WD2341+322	53.24±0.40	3	2,3,4	13000± 40	8.02±0.01	DA	24	H	0.62±0.01	11.55±0.04	−2.38±0.01	0.31±0.01	c,g
WD2352+401	45.12±0.36	2	2,3	7820± 180	8.04±0.04	DQ	31	He(+C)	0.60±0.03	13.21±0.03	−3.30±0.05	1.24±0.10	w

[a] The adopted parallaxes are weighted means in cases of multiple parallax determinations for a system. Model parameters were determined using these values. The Ref. column (4) identifies the source(s) of each parallax.

[b] WD cooling age only, not including main-sequence lifetime.

[c] M_V is determined from the best atmospheric model fit given that no apparent magnitude was measured in the V-band.

[d] No optical $BVRI$ photometry was obtained, thus, the SED was derived from standardized SDSS gri taken at the NOFS 1.3-m telescope on a photometric night. Photometric values are 15.42, 15.27, and 15.24 for gri, respectively.

[e] The best fit atmospheric model included [log He/H=-1.21].

[f] The best fit atmospheric model included [log H/He=-3.5], [log Ca/He=-10.21].

[g] No optical $BVRI$ photometry was obtained, thus, the SED was derived from SDSS $ugriz$ photometry extracted from DR12.

[h] Physical parameters are based on a single WD; however, there is evidence that this object is an unresolved binary and thus, a single star model does not accurately characterize the system.

[i] The best fit atmospheric model included [log C/He=−6.49].

[j] The best fit atmospheric model included [log C/He=−6.6].

[k] While no Balmer lines are present in the spectra, as pointed out by Giammichele et al. (2012), the Ca H & K lines are too sharp for a He-dominated atmosphere and thus, a pure-H model was adopted.

[l] The best fit atmospheric model included [log H/He=−3.5], [log Ca/He=−10.99].

[m] The best fit atmospheric model included [log H/He=−5.0], [log Ca/He=−9.26].

[n] The best fit atmospheric model included [log H/He=−3.7], [log Ca/He=−10.57].

[o] No satisfactory model fit was obtained, thus, derived parameters are likely unreliable.

[p] The best fit atmospheric model included [log C/He=−5.18].

[q] The best fit atmospheric model included [log C/He=−7.15].

[r] The best fit atmospheric model included [log H/He=−5.0], [log Ca/He=−11.25].

[s] The best fit atmospheric model included [log H/He=−5.0], [log Ca/He=−9.38].

[t] The best fit atmospheric model included [log C/He=−3.91].

[u] The best fit atmospheric model included [log H/He=−5.0], [log Ca/He=−8.63].

[v] Effective temperature is the limit of the model grid and for which additional pressure effects in this regime are not accounted.

[w] The best fit atmospheric model included [log C/He=−5.14].

References. — (1) this work (CTIOPI) π, (2) YPC (van Altena et al. 1995) π, (3) this work (NOFS) π, (4) *Hipparcos* (van Leeuwen 2007) π, (5) Lindegren et al. (2016) TGAS π, (6) Smart et al. (2003) π, (7) this work (CTIOPI) companion π, (8) Gatewood & Coban (2009) π, (9) Gianninas et al. (2015) π, (10) Debes et al. (2015) π, (11) YPC (van Altena et al. 1995) companion π, (12) *Hipparcos* (van Leeuwen 2007) companion π, (13) Lépine et al. (2009) π, (14) Ducourant et al. (2007) π, (15) Lindegren et al. (2016) TGAS companion π, (16) Aznar Cuadrado et al. (2004), (17) Bergeron et al. (1997), (18) Kawka et al. (2004), (19) Subasavage et al. (2008), (20) Limoges et al. (2015), (21) Subasavage et al. (2007), (22) Giammichele et al. (2012), (23) Dufour et al. (2007), (24) Gianninas et al. (2011), (25) Schmidt et al. (2001), (26) Debes & Kilic (2010), (27) Kawka & Vennes (2006), (28) Oppenheimer et al. (2001), (29) Zuckerman et al. (2003), (30) Farihi et al. (2011), (31) Dufour et al. (2005), (32) Ruiz & Bergeron (2001), (33) this work spectroscopy, (34) Sayres et al. (2012), (35) Lépine et al. (2005), (36) Koester et al. (2011), (37) Lépine et al. (2003), (38) Koester et al. (2005), (39) Scholz et al. (2002), (40) Koester et al. (1997), (41) McGraw & Robinson (1975).

Table 5
WD1242−105 Vital Parameters

Spectroscopic Results	
Period (days)	0.11885 ± 0.00056
q	0.685 ± 0.013
K1 (km s^{-1})	184.6 ± 2.3
K2 (km s^{-1})	126.5 ± 1.9
$\gamma 1$ (km s^{-1})	28.3 ± 1.7
$\gamma 2$ (km s^{-1})	44.8 ± 1.9
$\Delta\gamma$ (km s^{-1})	16.5 ± 2.2

Table 6
Contributions to the 25 pc WD Sample

Parallax Program	All π	$\pi_{\rm err} \leq 10\%$	Refs.
Yale Parallax Catalog	104	91	1
Hipparcos	5	5	2,3,4,5
Torino Observatory Parallax Program	2	2	6
Ducourant and Collaborators	1	1	7
Pre-2009 Sample	112	99	
Allegheny Observatory Parallax Program	4	4	8
Lépine and Collaborators	2	2	9
Gianninas and Collaborators	1	1	10
TGAS	2	2	11
Hipparcos Companion	1	1	12
CTIOPI	47	47	12,13
NOFS	20	20	12
CTIOPI and NOFS	3	3	12
Total	183[a]	179	

[a]As poor trigonometric parallax determinations, i.e., parallax error > 10%, are updated with robust determinations, their counts are removed from this total. At present, only four WD systems still have poorly constrained parallaxes.

References. — (1) van Altena et al. 1995, (2) van Leeuwen 2007, (3) Gould & Chanamé 2004, (4) Mugrauer & Neuhäuser 2005, (5) Chauvin et al. 2006, (6) Smart et al. 2003, (7) Ducourant et al. 2007, (8) Gatewood & Coban 2009, (9) Lépine et al. 2009, (10) Gianninas et al. 2015, (11) Lindegren et al. 2016, (12) this work, (13) Subasavage et al. 2009.

TABLE 7
25 PC WD SKY DISTRIBUTION

Declination Range	# of Systems	# of New Systems
+90° to +30°	33	9
+30° to +00°	37	11
Total (North)	**90**	
−00° to −30°	28	13
−30° to −90°	28	20
Total (South)	**89**	